Clockwork Orangutan: microRNAs, thermoregulatory tradeoffs, and the evolution of brain size.

Bastian Fromm*, PhD

The Arctic University Museum of Norway

UiT- The Arctic University of Norway 9037

Tromsø, Norway

Thomas Sorger, PhD

Department of Biology

Roger Williams University

Bristol, Rhode Island 02809, USA

*** corresponding author**

SUMMARY

Current hypotheses to account for the energy demand associated with the disproportionate increase in brain size in the human lineage have not considered thermoregulatory constraints. Unlike log-based specific metabolic rates (*sMR*s), the distribution of cellular *MR*s (*cMR*s) can be matched to those of relevant traits, like body temperature or the number of microRNA families (*mirFam*). We demonstrate that the *mirFam*-based *cMR*s of the four most thermogenic organs (kidney, heart, liver and brain) form a core with a joint *cMR* that scales as $M^{0.53}$, close to that predicted by a comprehensive biophysical model of thermoregulation in homeotherms. Across Euarchontoglires, core organs do not evolve independently: while all organ sizes increase with body size, brain and liver proportions in the core are strictly anti-correlated, as are their *cMR*s, echoing the expensive tissue hypothesis. We propose a positive feedback relationship between larger brain size and greater reliability of the energy supply, on the one hand, and decreasing reliance on liver gluconeogenesis, on the other. The corresponding logistic model detects size adaptation to a low-energy regime among the smallest primates and, among primates with the largest brains, thermoregulatory adaptation to the limit on the rate of heat dissipation.

INTRODUCTION

The diversification of mammalian orders has been characterized by two general trends, increasing size (Baker et al, 2015) and decreasing body temperature (Avaria-Llautureo et al, 2019). Variation in resting metabolic rate (*rMR*)[1], in contrast, did not exhibit a long-term trend but, in conjunction with the variation in thermal conductance (C_{min}), has allowed mammalian species across the entire range of size to occupy nearly the entire range of climatic zones (Fristoe et al, 2015). Importantly, this coordination occurs between the mass-independent variation (*i.e.* residuals) of *rMR* and C_{min} (Naya et al, 2013; Fristoe et al, 2015). Taken together, the anticorrelation between body size and temperature, and the complementarity between *rMR* and C_{min}, conform to a physiological limit on the rate of heat dissipation, initially proposed by Speakman and Król (2010). This thermoregulatory constraint has been inferred from the much narrower range of mammalian tolerance to heat than to cold (Araujo et al 2013; Khaliq et al, 2014; Bennett et al, 2021; Fromm and Sorger, 2023). Despite this evidence, current accounts of the adaptations associated with the disproportionate increase of brain size and heat production in the human lineage have not considered thermoregulatory constraints (for review, see Heldstab et al, 2022).

In humans, the brain's power consumption of 15W raises the temperature of its venous outflow by ~ 0.2 - 0.3ºC (Nybo et al, 2002; Nybo, 2012; Wang et al, 2014; Sung et al, 2022; for reviews see Claassen et al, 2021 and Travers et al, 2022). Given that ~ 15% of human blood volume perfuses the brain every minute (Lassen, 1985), this suggests a significant thermoregulatory challenge: orangutans are similar to humans in body size, but their brains are ⅔ smaller and generate only 4W heat (Pontzer et al, 2016).

[1] *rMR* is used here to include *MR* measurements obtained under basal conditions.

There are two ways to account for the maintenance of temperature homeostasis, given such a difference in the rate of heat production: either by a significant adjustment in thermal conductance, or by a tradeoff in energy expenditure with another metabolically expensive tissue, such as kidney, heart, liver or intestine (Aiello and Weaver, 1995). Apart from hairlessness and bipedalism, humans exhibit no adaptation for heat dissipation that is not shared by other great apes (Walters et al, 2004; Notley et al, 2024); like chimpanzees (Lindshield et al, 2021), early hominids most likely relied primarily on behavioral thermoregulation, which does not address the problem of internal heat generation. Despite numerous attempts, the effort to detect the tradeoff predicted by the "expensive tissue hypothesis" has been largely abandoned since the publication of a large study by Navarette et al (2011), which encompassed eight organs in 100 species, including 23 primates. However, as we detail below, such a tradeoff cannot be detected by conventional brain-body allometry, the method that has been used since the seminal analysis by Lande (1979) (see, for example, Burger et al, 2019 and Smaers et al, 2021).

Mammalian organ sizes are proportional to body size (Gallagher et al, 1998; Wang et al, 2012), independent of phylogenetic relatedness (Antol and Kozlowski, 2020), and therefore they are also proportional to each other (Gallagher et al, 1998). Navarette et al (2011) found no significant anticorrelations between brain size and those of seven other organs in primates, even among their mass-independent residuals. We postulated that the four most thermogenic organs (kidney, heart, liver and brain) constitute a thermoregulatory core, as described in the comprehensive biophysical model of Porter and Kearney (2009). We found that evolutionary increases in the relative proportion of the brain *in this core* were offset by decreases in the relative proportion of the liver, an anticorrelation that depended on their mass-independent residuals. We then estimated the cellular *MR* (*cMR*) of each core organ, based on three criteria:

a) size-independent correlation with *mirFam* (physiological relevance) (Fromm and Sorger, 2023);
b) correspondence of the combined *cMR* of these organs with that of the thermogenic core predicted in the biophysical model of Porter & Kearney (2009) (thermodynamic relevance);
c) utility for the unsupervised classification of major primate clades (phylogenetic relevance).

The joint *cMR* of this 4-organ core scaled as $M^{0.53}$, close to that predicted for the thermogenic core of homeothermic endotherms (Porter and Kearney, 2009). Examining the evolutionary variation of these *cMR*s across 51 Euarchontoglires, we found that liver *cMR*s were anticorrelated with body size and the *cMR*s of kidney, heart and brain

Since the liver is the primary organ of gluconeogenesis in fasting or starvation, the liver-brain anticorrelations with respect to mass and *cMR* conform to an energy-based, positive feedback model of brain size evolution (Heldstab et al, 2022). We demonstrate that a logistic model of the relationship between brain size and energy reliability supports the inference of size adaptation to a low energy

regime by reduction in size, on the one hand, and thermoregulatory adaptation to the physiological limit on the rate of heat dissipation (hence rate of thermogenesis) in large-brained primates, on the other.

RESULTS

T*he proportion of brain mass in the core varies reciprocally with that of liver*

Of the six possible tradeoffs In a core consisting of four thermogenic organs, one major trade off occurred consistently among primate clades, that between brain and liver (Figure 1A, B). A dampened tradeoff between heart and kidney occurred approximately “in phase” with the major tradeoff. Brain and liver proportions in the core also varied reciprocally across 30 additional Euarchontoglires, together with a diminished reciprocity between heart and kidney (Supplementary Figure S1).

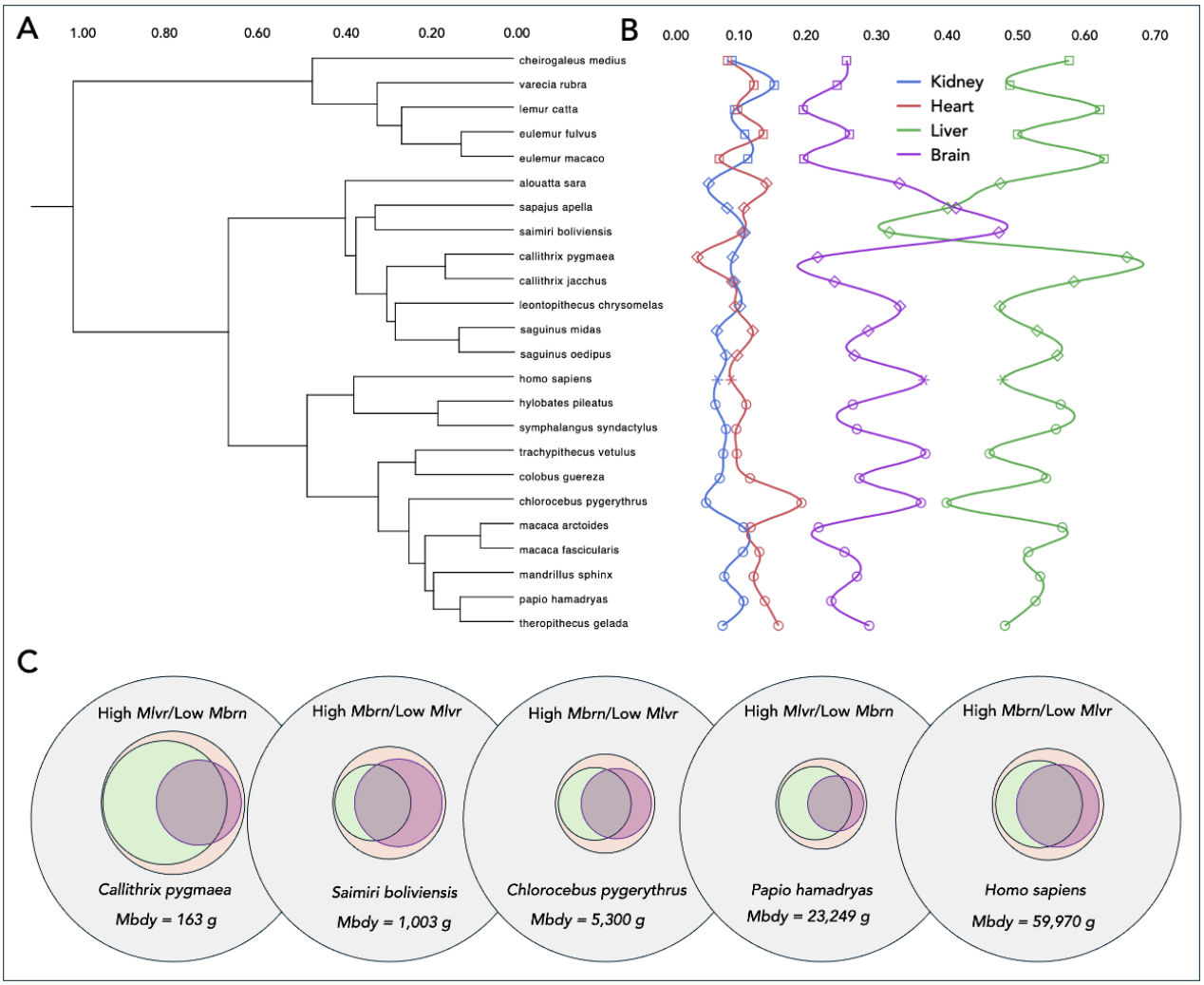

Figure 1. The proportion of brain mass in the thermogenic core varies reciprocally with that of the liver.
A. Time tree of 24 primates (scale bar represents the relative time of divergence).
B. Mass proportion of each organ relative to the total core mass.
C. Summary model comparing representative species with low or high ratios of brain/liver mass. The radius of each circle represents a spherical volume corresponding to organ or core mass, scaled to body size (*Mbdy*: equal circle diameters). The relative proportions of liver and brain are represented by green and purple circles, respectively.

The variation in liver and brain proportions is summarized geometrically in Figure 1C. Relative core size (~ $M^{0.50}$) is predicted to decrease with body size (~ $M^{0.75}$) (Porter & Kearney, 2009), but owing to the size of the human brain, relative core size is greater than that found in baboons, which have less than half of the body mass of humans.

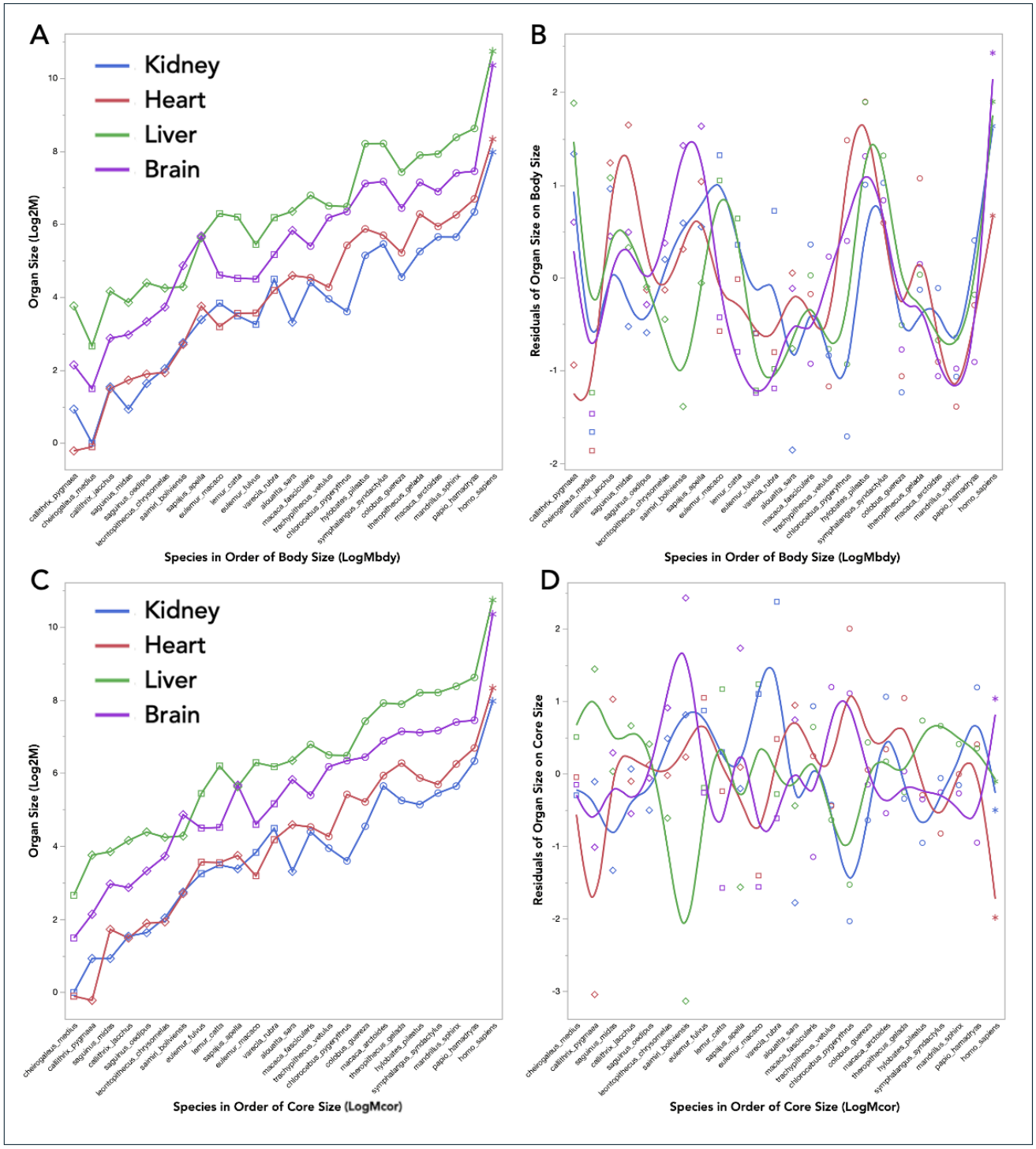

Figure 2. The reciprocal variation between liver and brain mass is a function of total core size.
A and C: Variation of organ size relative to body size and core size in primates.
B and D: Mass-independent residual variation relative to body size and core size in primates.

Tradeoffs between liver and brain masses are readily demonstrable with log-transformed data, *provided that they are ranked according to core size* (Figure 2C)*, not body size* (Figure 2A). Examination of the residuals of the corresponding regressions revealed a periodic pattern of variation for each organ, corresponding to their relative proportion of body mass (Figure 2B) or core mass (Figure 2D). The periodicity is a function of autocorrelation, a feature of any part/whole comparison, which can be easily demonstrated when the analysis is limited to a single pair of organs (Supplementary Figure S2). Since the tradeoff between the residuals of brain and liver mass is apparent only when standardized against core mass (Figure 2D versus Figure 2B), standardization of log *Mbrn* against log *Mbdy* would preclude its detection (*e.g.* Navarette al, 2011).

The evolution of thermal conductance has generally been investigated in the context of adaptation to ambient temperatures, which is the outcome of adjustments to both thermal conductance and resting *MR* (Scholander et al, 1950; Naya et al, 2013; Khaliq et al, 2014; Fristoe et al, 2015). While thermogenesis is a core organ property, thermal conductance depends on total surface area and, like organ size, is expected to increase geometrically with body size, as well as with ambient temperature.

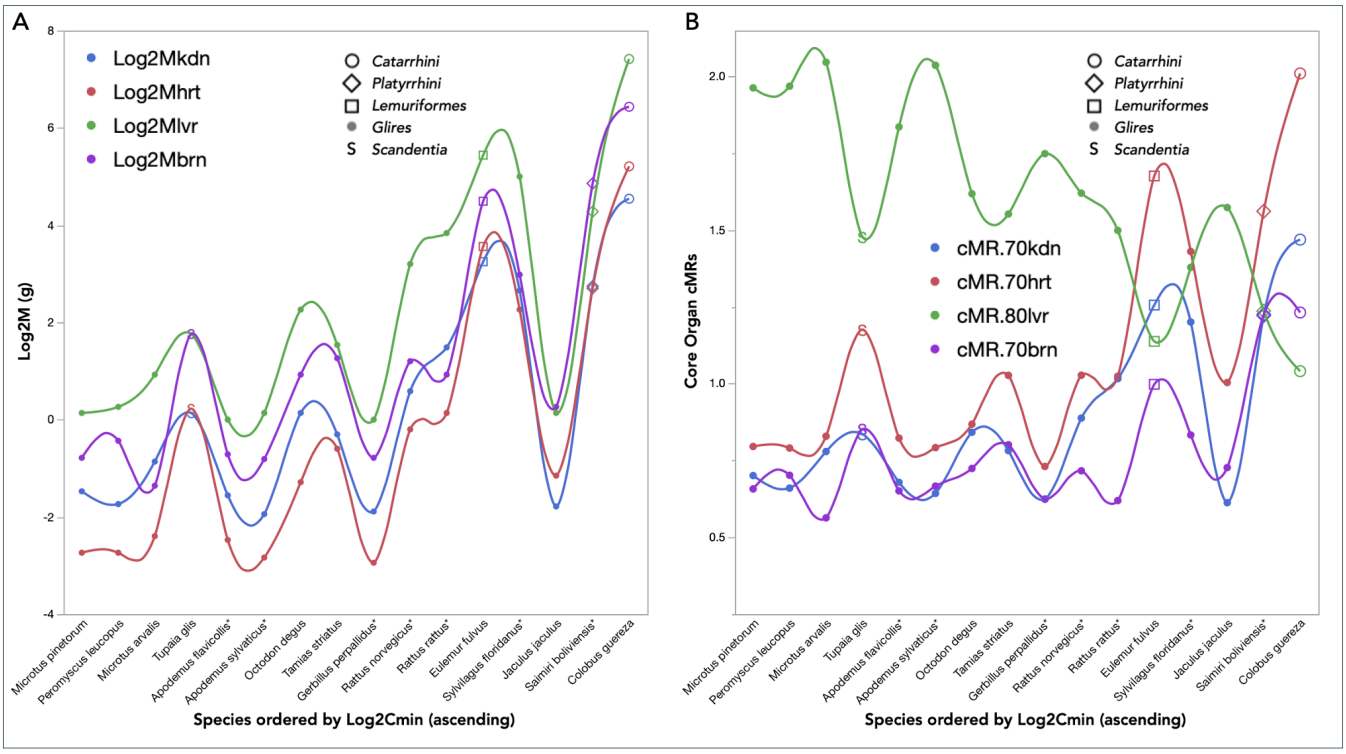

Figure 3. Thermal conductance also covaries with *cMR* tradeoffs between liver and brain.
A. Thermal conductance is a direct function of whole body size, and therefore of organ size.
B. The size-related increase in thermal conductance is related to a compensatory tradeoff in core thermogenesis between liver, on the one hand, and kidney, heart and brain, on the other.
Asterisks (*) represent species in the 4-organ dataset of Wang et al (2012) that have been substituted for congeneric species in the C_{min} dataset of Khaliq et al (2014).

For example, in a subset of 16 species from the Wang dataset for which C_{min} values were available (Khaliq et al, 2014), $\sqrt{Mbdy}$, $\sqrt{Mcor}$ and $\sqrt{Mbrn}$ predicted 67 - 70% of the variation in $\sqrt{C_{min}}$, respectively (6.96e-05 > P > 3.40e-05, or 52 - 58% of the variation when using log-transformed values). As shown in Figure 3, thermal conductance was highest among primates and the largest Glires, and was not associated with tradeoffs in organ mass (Figure 3A), but rather with tradeoffs between liver *cMR* and the *cMR*s of kidney, heart and brain (Figure 3B), estimated as described below.

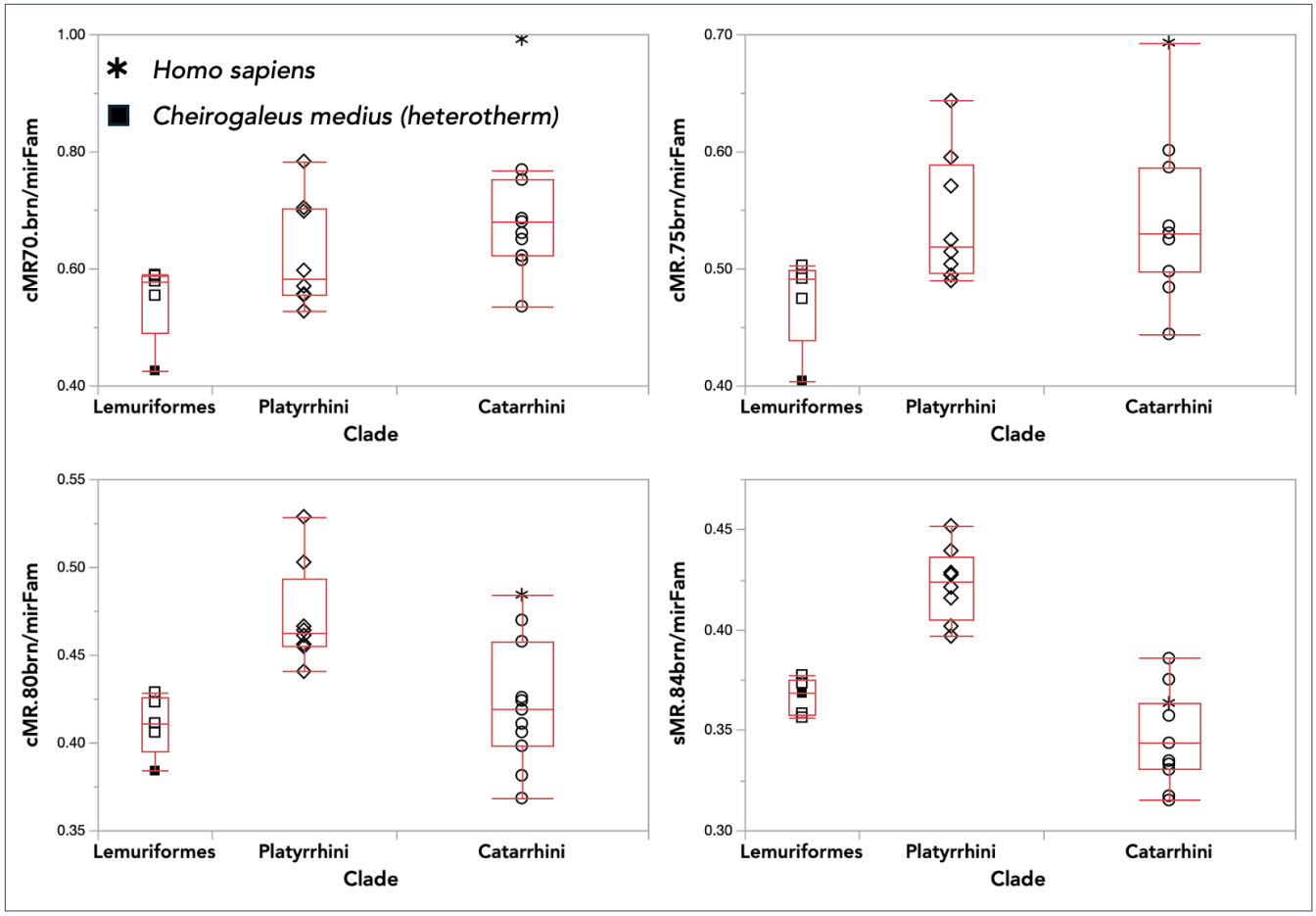

Figure 4. Comparison of the distribution among 24 primates of the ratio to *mirFam* of the log-based brain *sMR* (*sMR.84brn*/*mirFam*) with those of *cMR.70brn*, *cMR.75brn* and *cMR.80brn*.

Physiologically-based cMRs do not correspond to log-based sMRs

Assuming a power law model, we distinguish between

specific *MR*s (*sMR*s): $sMR = m \times M^b$,

where b is the slope of log *rMR*/log *M*, and

cellular *MR*s (*cMR*s): $cMR = n \times M^c$,

where c is the allometric exponent obtained by maximum likelihood fitting of rMR/M^c to the distribution of a physiologically-relevant trait, such as *mirFam* (Fromm and Sorger, 2023). Unlike *sMR*s, *cMR*s obtained by fitting rMR/M^c to the distribution of *mirFam* are sensitive to body temperature and robust to sample differences in the range of mass (Fromm and Sorger, 2023). For example, when scaled to

cMR.70, the brain *cMR.70*/*mirFam* ratios of the human and the dwarf lemur, a heterotherm, occupied the top and bottom of the distributions of species in their respective clades. However, when scaled to the slope of the ratio of log *rMR*/log*M* (*sMR.84*), the corresponding ratios were near the middle of ranges of their respective clades (Figure 4).

Rates of cellular metabolism depend on traits that do not scale logarithmically, such as body temperature (T_b) or the rate of protein synthesis, which will vary by tissue type and differ between tissues that are renewable or post-mitotic. The net rate of protein synthesis, which drives 20% of cellular *MR* (Buttgereit et al, 1995), depends on the global rate of repression by microRNAs (Baek et al, 2008; Selbach et al, 2008), for which the species-specific number of microRNA families (*mirFam*) may serve as a proxy (Fromm and Sorger, 2023). Thus, while the rank order of log-based *sMR*s, and therefore of *sMR*/trait ratios, is fixed according to species size, the rank order of *cMR*s is matched to non-logarithmic traits by variable allometric scaling, yielding biologically meaningful slopes for these relationships and meaningful rank orders for *cMR*/trait ratios. These attributes have obvious implications for models of genetic and phenotypic covariance (Lande, 1979; Felsenstein, 1985; Hansen, 1997; Pagel, 1999; Svensson et al, 2021; Walter and McGuigan, 2023).

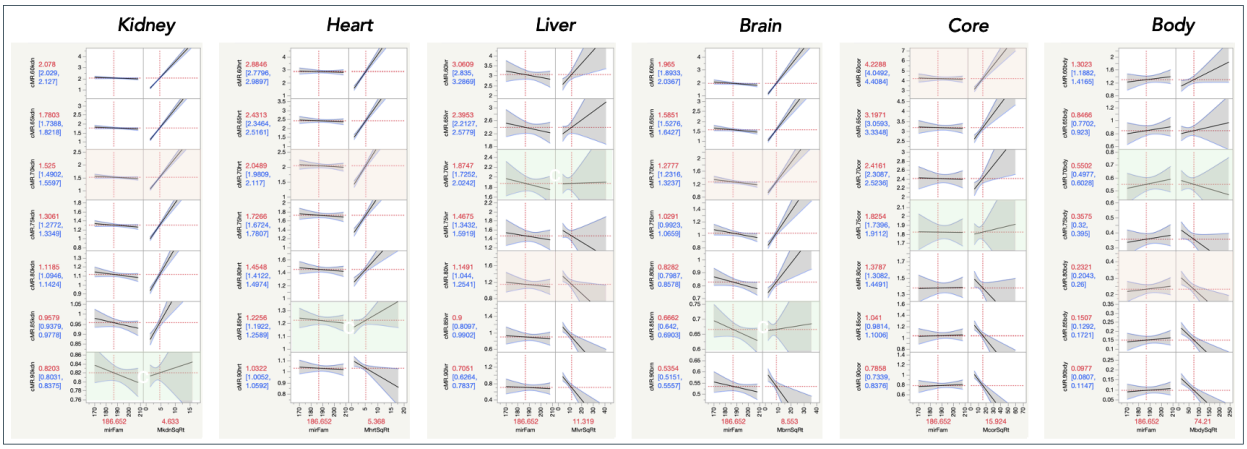

Figure 5. Dependence of *cMR* on √*Morg* and *mirFam* in 22 primates.
√*M*, a natural scale for *cMR*s, yielded *P* values several orders of magnitude lower than did a log scale. Estimated *cMR* slopes are shaded pink, whereas log-based *sMR* slopes are shaded green. Note that the correlations with *mirFam* parallel the correlation with body mass, and that *sMR* slopes correspond to crossover points for the inversions of the *cMR* slopes. Values in red represent means (± CI).

Estimation and physiological relevance of thermogenic organ cMRs

We have previously presented evidence that the number of microRNA families is a statistically and mechanistically credible proxy for the global rate of protein synthesis, hence cellular *MR* (Fromm and Sorger, 2023). We further showed that *mirFam* is an attractor for whole animal *cMR* across the major mammalian clades (Monotreme, Atlantogenata, Laurasiatheria and Euarchontoglires) in a model of stabilizing selection (Fromm and Sorger, 2023). Phylogenetic regression in conjunction with variable

allometric scaling, yielded $M^{0.71}$ as the optimal allometric scaling of *cMRbdy* with respect to *mirFam* across 10 representative mammals (R^2 = 0.78, P = 4.55e-04), while $M^{0.75}$ was the optimal allometric scaling of *cMRbdy* in the model of stabilizing selection (Fromm and Sorger, 2023). As a starting point for the estimation of *mirFam*-based *cMR*s for each of the four thermogenic organs, we compared the dependence of *cMR*s between *cMR.60* - *cMR.90* on *mirFam* and organ mass (Figure 5). Assuming an operating range of $M^{0.70}$ - $M^{0.80}$, we chose the organ *cMR* yielding the lowest P value for the multiple regression, hence *cMR.70kdn*, *cMR.70hrt*, *cMR.70brn* and *cMR.80lvr*.

Plotting these *cMR*s as a function of primate body size revealed that the strong anticorrelation between liver *cMR.80* and the *cMR.70*s of the other core organs appears to be essential to establishing an overall negative slope of *cMR.75bdy* with respect to animal size (Figure 6A). We obtained similar slopes plotting organ *cMR*s against thermal conductance ($\log_2 C_{min}$) among 16 Euarchontoglires (Figure 6B), consistent with a common basis for these physiological and thermoregulatory relationships.

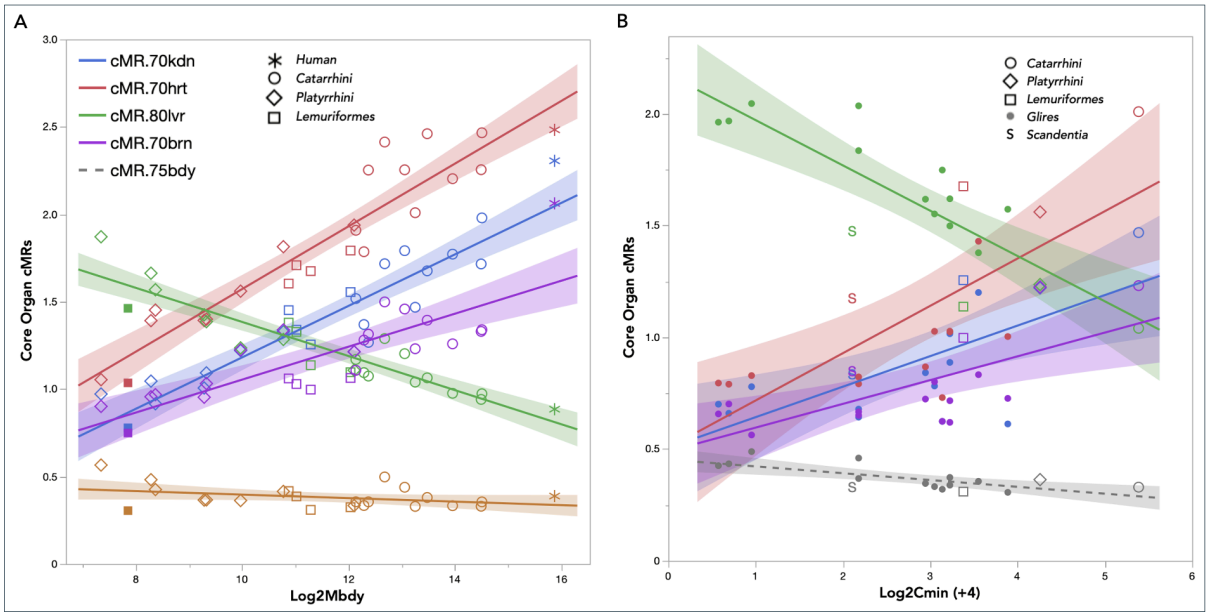

Figure 6. Core organ *cMR*s as a function of body size and thermal conductance.
A. Primates (N = 24). Filled symbols represent heterotherms.
B. Euarchontoglires (N = 16). Shaded bands: confidence interval for each regression line.

We then tested the credibility of this combination of core *cMR*s with respect to thermodynamic and phylogenetic models. For a steady state (whole animal) resting *MR* that scales as $M^{0.75}$, the rate of core thermogenesis is predicted to scale as ~ $M^{0.50}$ (Porter & Kearney, 2009). We used partial least squares regression (de Jong, 1993) to predict the allometric scaling of theoretical "*cMRcor*"s consisting of linear combinations of either the *mirFam*-based *cMR*s, or the log-based *sMR*s, of the four thermogenic organs:

$$cMR.Xcor = (rMRkdn + rMRhrt + rMRlvr + rMRbrn) / (Mkdn + Mhrt + Mlvr + Mbrn)^X$$

$$= (a \bullet cMR.70kdn) + (b \bullet cMR.70hrt) + (c \bullet cMR.80lvr) + (d \bullet cMR.70brn)$$

OR

$$cMR.Xcor = (rMRkdn + rMRhrt + rMRlvr + rMRbrn) / (Mkdn + Mhrt + Mlvr + Mbrn)^X$$

$$= (a' \bullet sMR.86kdn) + (b' \bullet sMR.94hrt) + (c' \bullet sMR.67lvr) + (d' \bullet sMR.86brn)$$

In the latter case, we applied the slopes derived from the regressions of log *rMR* versus log *Mcor*, which detected tradeoffs between the residuals for log *Mlvr* and log *Mbrn* (Figure 2C, D). Peak R^2 values for both sets of models occured on either side of the crossover for the inversion of slopes representing the core *cMR* dependence on size and *mirFam* (Figure 7A). In both cases, the optimal allometric scaling of the predicted *cMRcor*'s was $M^{0.53}$, close to the predicted scaling of a thermogenic core in the ellipsoid homeotherm model (Porter and Kearney, 2009), with a 6% higher value of R^2 value for the *cMR* model, compared with the *sMR* model (Figure 7A).

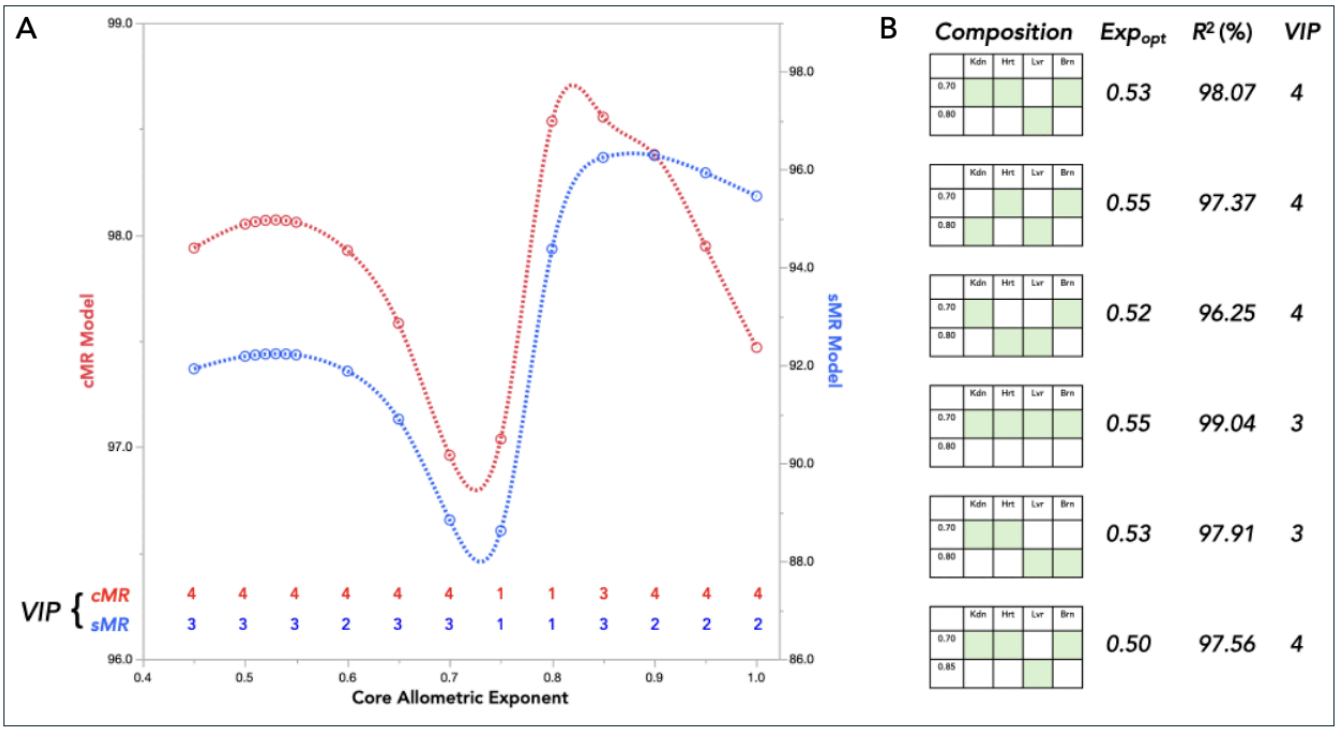

Figure 7. R^2 (% variation) for models of *cMRcor* predicted by linear combinations of *mirFam*-based *cMR*s or log-based *sMR*s of the four thermogenic organs (note the difference in scales; $N = 22$). A. Comparison between *mirFam*-based organ *cMR*s and log-based organ *sMR*s. *VIP* (*variable importance of projection*) values indicate the number of organs upon which each model depends. B. Comparison of combinations of *cMR.70* and *cMR.80* among the four thermogenic organs. Exp_{opt}: the optimally fitting core allometric exponent for the linear model.

In the context of the evolution of thermoregulation, the coefficients of the individual organ *cMR*s in the optimal model may be interpreted as reflecting the relative degree of evolutionary constraint:

$$\textbf{\textit{cMR.53}cor} = 0.53 \bullet \textbf{\textit{cMR.70kdn}} + 0.69 \bullet \textbf{\textit{cMR.70hrt}} + 0.37 \bullet \textbf{\textit{cMR.80lvr}} + 0.09 \bullet \textbf{\textit{cMR.70brn}}$$

In addition to the higher range of R^2 values for the *cMR* models compared to the sMR models, there was a critical difference in their *VIP* statistics (variable importance of projection) (Wold et al, 1993). The *VIP* statistic can be interpreted as the degree of interdepence among variables that is constraining the model. Over the range *cMR.45cor* - *cMR.70cor*, the *cMR* model depended significantly on all four organ *cMR*s, while the *sMR* model depended only on three (excluding liver) or two organ *sMRs* (excluding liver and brain) (Figure 7A, bottom), contrary to the notion of a thermogenic core. Significantly, at *cMR.75cor*, the linear *cMR* model depended only on a single variable, *cMR.80lvr*, which lends further support to the notion of minimal constraint on the composition of the core when scaled to $M^{0.75}$, and highlights the importance of liver *cMR* in dictating the overall rate of thermogenesis.

In addition to comparing the *cMR* and *sMR* models, we varied the combinations of individual organ *cMR*s between *cMR.70* - *cMR.85* (Figure 7B) and found that of the four models that depended on all four organ *cMR*s (*i.e.VIP* = 4), the two combinations with the highest R^2 values were:

[*cMR.70kdn*, *cMR.70hrt*, *cMR.80lvr* *or* ***cMR.85lvr,* and *cMR.70brn*]**.

In order to distinguish between these two models using a different criterion, we predicted that a physiologically relevant set of core organ *cMR*s would be useful in the unsupervised classification of major primate clades. Expectation maximization of Gaussian (normal) mixture models allows the inference of such a latent grouping variable (Dempster et al, 1977; Celeux and Govaert, 1995). After varying the *cMR*s for the liver between *cMR.75* - *cMR.85*, the combination of *mirFam*-based *cMR*s estimated originally also yielded the lowest information criterion (Supplementary Figure S3):

[c*MR.70kdn*, *cMR.70hrt*, *cMR.80lvr*, *cMR.70brn*].

The evolution of tradeoffs of organ cMRs conforms to the core model of thermoregulation. The evolutionary histories of the four organ *cMR*s provided compelling evidence that they have been constrained by their relationship to the core. We examined how the tradeoffs between brain and liver *cMR*s were related to the divergence of orders and species of Euarchontoglires, and to the corresponding changes in body size (Figure 8).

Generally opposing directions of evolution were observed between body size and *cMR.80lvr*, and within each tree between Catarrhini and Glires (Figure 8). An accelerated increase in liver *cMR* accompanied the decrease in size of the two smallest of the Platyrrhini, one of which (*Callithrix pygmaea*) is suspected to be heterothermic (Tattersall, 2012). All five of the smaller (< 1.0 kg) Platyrrhini exhibited elevated levels of *cMR.80lvr*, consistent with adaptation to a low energy regime and increased reliance on gluconeogenesis. Among Glires overall, those species that underwent the greatest reductions in size exhibited the highest increases in liver *cMR.80*, while the largest Glires (Lagomorphs) exibited the lowest liver *cMR*s (Figure 8).

Brain *cMR.70* accelerated and increased in intensity with the divergence of Haplorrhini, and again in the case of humans, in contrast to its relative stasis in Lemuriformes and Glires (Figure 8). Compared to their ancestor, the five smallest Platyrrhines underwent an accelerated *reduction* in brain *cMR*, a clade-wide tradeoff that mirrored the size-related tradeoff in Glires between liver and brain *cMR*s.

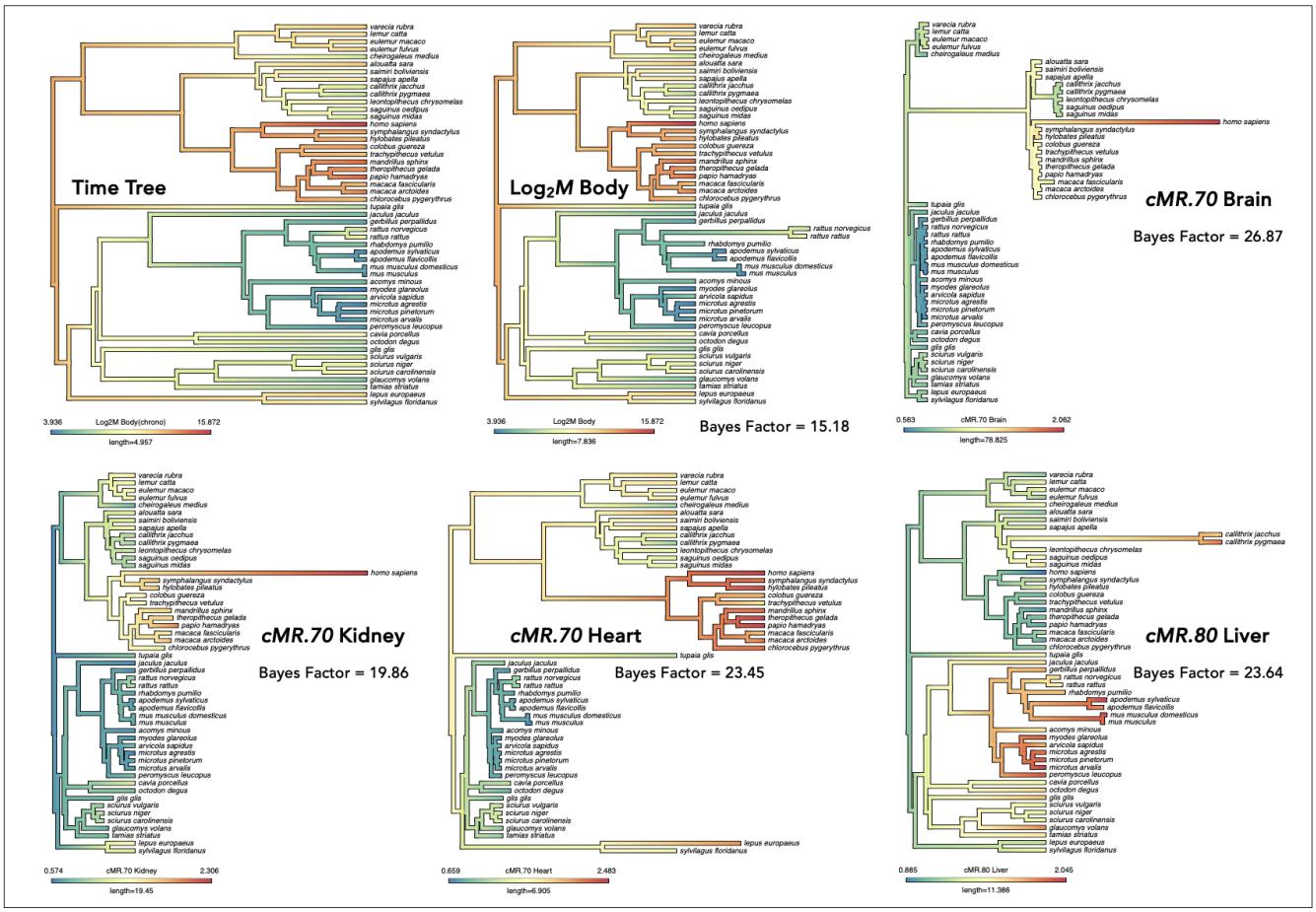

Figure 8. Variable rate phenograms of *Log$_2$M*, *cMR.80lvr*, and *cMR.70* of kidney, heart and brain. Bayes factors were computed from the difference between the median log likelihood (*Lh*) of the 1% most likely trees and the median *Lh* of the 1% of trees with the smallest non-zero sum of changes to branch length, *i.e.* those trees most similar to the reference time tree.

The relative levels and evolutionary rates of heart *cMR.70* generally tracked body size, with two notable exceptions: the accelerated rates of heart evolution in the largest clades of both Glires (Lagomorpha) and primates (Catarrhini) (Figure 8). In addition to *cMR.70brn*, humans exhibited an exceptional increase in the rate of evolution of kidney *cMR.70*, potentially associated with adaptation to a diet enriched in protein (Simmen et al, 2017; Paine et al, 2019; Grabowski et al, 2023) or adaptation to an altered landscape of opportunities for hydration *versus* risks of dehydration ("Savanna hypothesis") (Dart, 1925; Mascia-Lees et al, 1986; Reed, 1997; Staubwasser et al, 2018; Paine et al, 2019; Davies et al, 2020; Lindshield et al, 2021; Zeller et al, 2023). A massive simulation of 2 million years of African and Eurasian climate and habitats indicated that the evolution *H. sapiens* from *H. heidelbergensis* in southern Africa occurred during an unusually warm period that required adaptation to hotter, drier conditions (Timmermann et al, 2022).

DISCUSSION

The recent addition of hundreds of primate genome sequences (Kuderna et al, 2024) has been accompanied by ever more fine-grained studies of the phylogenetic covariance of traits suspected to influence the evolution of brain size, such as changes in diet and/or gains in the efficiency or reliability of the acquisition and assimilation of food, storage of energy reserves, gestation, lactation and infant care (Mascia-Lees et al, 1986; Koteja, 2000; Fonseca-Azevedo and Herculano-Houzel, 2012; Isler and van Schaik, 2012; Isler and van Schaik, 2014; Kuzawa et al, 2014; Pontzer et al, 2016; Simmen et al, 2017; Grabowski et al, 2023). For the reasons elaborated above, we submit that a fundamental assumption underlying these analyses – that log-transformed brain mass provides an accurate ranking of the rates of brain energy expenditure – is not justified. Simply put, the distributions of *sMR*s inferred from ratios of brain log *rMR*/log *M* cannot be related to the distributions of relevant physiological and thermodynamic variables.

Countless comparative studies of the evolution of whole body *rMR* in mammals have yielded allometric exponents of approximately 0.75 for log-based *sMR*s (Kleiber, 1932; Ballesteros et al, 2018). In this study, *sMR* slopes corresponded to the crossover points for the inversion of *cMR* slopes with respect to *mirFam* and organ size, and therefore to the zone of weakest association and constraint by these factors. In this study, only a core composed of the four most thermogenic organs had an *sMR* slope near to $M^{0.75}$ ($M^{0.756}$), suggesting that evolutionary conservation of 3⁄4 power allometry is related to selection primarily on the composition of the core, hence the rate of internal heat generation, and only secondarily on body mass or *rMR* (White et al, 2019). This interpretation is further supported by the observation that a linear model of *cMR.75cor* depended on the *cMR* of only a single organ, the liver, while the optimal core *cMR* model (*cMR.53cor*) depended on the *cMR*s of all four thermogenic organs.

Of the six possible tradeoffs in *cMR* among the four thermogenic organs, why is the brain-liver tradeoff the most significant? During the postabsorptive or fasting state, the liver is the primary organ of gluconeogenesis: the glucagon-dependent reduction of amino acid or glycerol carbons, fueled by free fatty acids released from adipose tissue. Gluconeogenesis contributes 40 - 60% of total glucose production after an overnight fast, and greater than 90% after 48 hours of fasting (Chung et al, 2015). The oxidation of fatty acids also generates ketone bodies, which can supply up to 60% of the human brain's energy supply during a prolonged fast, thereby sparing muscle protein (Owen et al, 1967; Garcia-Rodriguez and Giménez-Cassina, 2021). Evidence from both human ontogeny and the phylogeny of Euarchontoglires indicates that gluconeogenesis has played a pivotal role in a tradeoff between the rates of brain and body growth.

The rate of glucose utilization peaks around age 5 in humans, early in the extended period between weaning and sexual maturity, corresponding to the slowest rate of increase of body mass (Kuzawa et al, 2014). Based on the turnover of isotopically-labeled glucose, glucose production was proportional to brain mass over the entire lifespan, and therefore highest among young children (Bier et al, 1977). Among preubertal children (7 - 9 years of age), the rate of gluconeogenesis was still 50% higher than that found among adolescents (Sunehag et al 2001; Sunehag et al 2002).

Drawing on metabolite fluxes measured in humans, Kummitha et al. (2014) developed a computational model of the corresponding fluxes in mice and found that after an overnight fast, the rates of liver gluconeogenesis, lipolysis and proteolysis were all elevated ~ 10-fold in mice, relative to the corresponding rates in humans. This comports well with our observation of opposite directions of evolution of *cMR.80lvr* between Glires and primates, associated with opposite strategies for body size and reproduction (Jeschke and Kokko, 2009). If an evolutionary increase in reliability of the energy supply meant a decrease in the frequency or duration of fasting, hence reliance on gluconeogenesis, then retention of ancestral relative liver size and *cMR* would have been inefficient. Such a dynamic would have been reinforced if brain enlargement routlinely led to greater energy security.

The following *cMR*-based model of brain size evolution posits a simple feedback loop between brain size and the reliability of the energy supply: improvements in energy reliability facilitate increases in brain size, which in turn favor further improvements in energy reliability, up to the limits imposed by anatomy and physiology, such as the diameter of the birth canal and the physiological limit on the rate of heat dissipation (Speakman and Król, 2010; additional details below). It is a classic logistic model, with cMR_{max} standing in for carrying capacity in a population logistic model:

$$\mathbf{d}(\boldsymbol{cMRbdy}) \,/\, \mathbf{d}(\boldsymbol{Vbrn}^*) = \boldsymbol{r} \bullet \boldsymbol{cMRbdy}\,[1 - (\boldsymbol{cMRbdy} \,/\, \boldsymbol{cMRbdy}_{max})]$$

where ***Vbrn**** is the log ratio of endocranial volume to body mass, ***r*** represents the growth rate, and the range of ***cMRbdy*** has been scaled to 1.0.

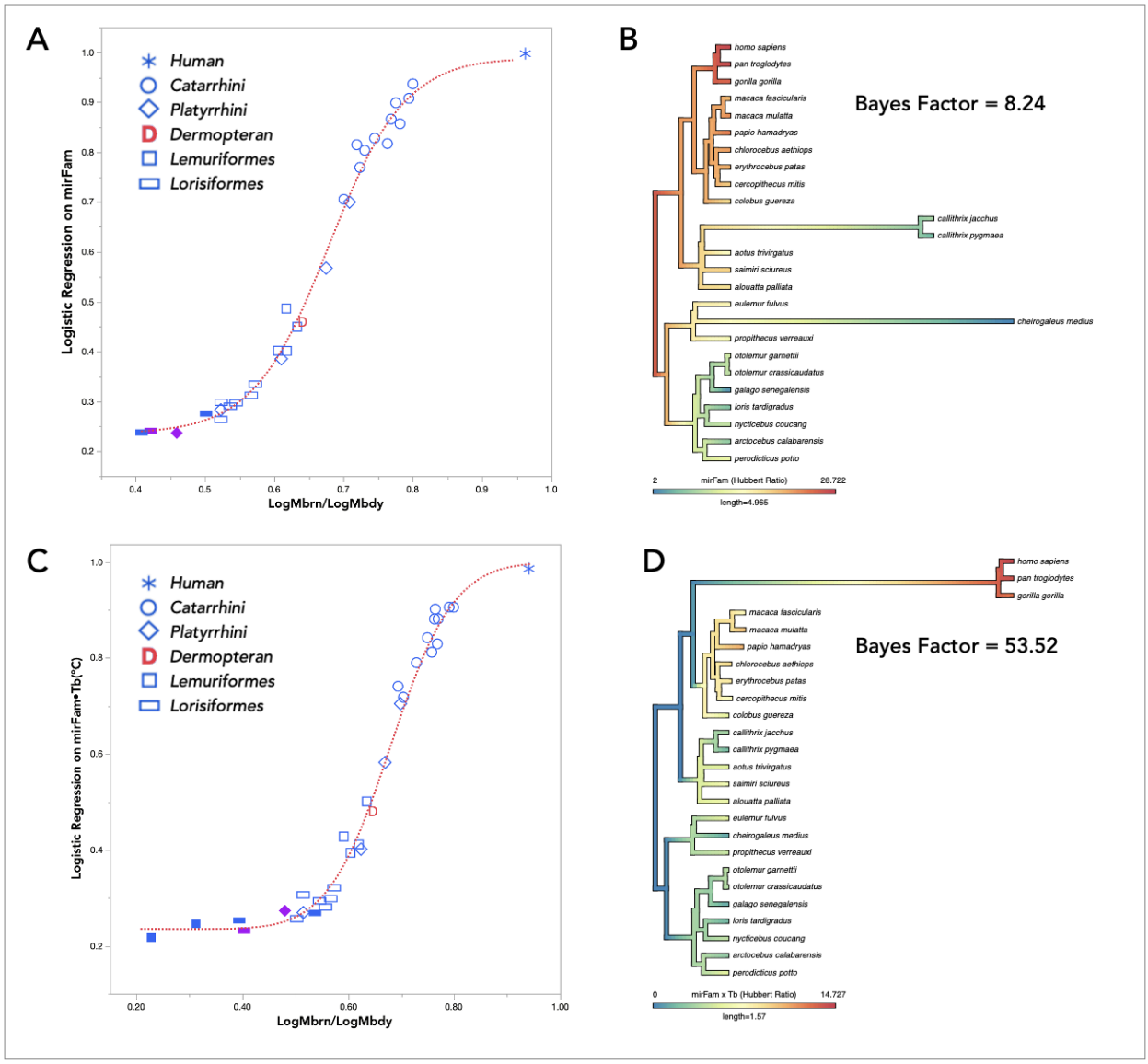

Figure 9. Logistic models of brain size evolution (data from Grabowski et al, 2023).
A, C. For these idealized models (R^2 = 1.00), *mirFam* or *mirFam•*T_b(ºC) was that predicted by the original logistic regression model (original R^2 = 0.90 and 0.86, respectively) (jitter applied).
Filled symbols: heterotherms (blue), suspected heterotherms (purple). D = *Galeopterus variegatus*.
B, D. Variable rate phenograms of the Hubbert linearization of the logistic functions.

This neutral model reduces several current hypotheses (Expensive Brain/Ecological Brain/Cognitive Buffer) (Heldstab et al. 2022) to one that does not presuppose any underlying mechanism. We applied this model to the primate brain size dataset of Grabowski et al (2023), fitting it to *mirFam*, a proxy for *cMRbdy*, *i.e.* the overall rate of energy utilization (Fromm and Sorger, 2023) (Figure 9A). Unexpectedly, the model revealed that relative brain size is a predictor of *mirFam*, rather than *vice versa*, lending

credence to the proposition that larger brains were associated with improvements in the reliability of the energy supply.

Given that the relative sizes of the three other thermogenic organs also fit logistic models for *mirFam* (Supplementary Figure S4), the question arises as to which relationship is the principal driver of adaptation. In phylogenetic regressions for organ *cMR*s ranging from *cMR*.60 - *cMR*.80, kidney, heart and liver *cMR*s varied independently of phylogeny (Pagel's *lambd*a = 0), while the variation of brain *cMR*.60 - *cMR*.80 with respect to *mirFam* was secondary to phylogenetic distance (Pagel's *lambda* = 1.0 in each case), indicating that the divergence of primate species largely coincided with changes in the relationship of *mirFam* to brain mass and *cMRbrn* (Supplementary Table S3) (Pagel, 1999).

Returning to the logistic model based on relative brain size, a variable rate phenogram for primate species was generated using the ratios from a Hubbert linearization of the logistic function (Figure 9B) (Hubbert, 1982). Thus, the color scale represents the rank on the logistic curve which, in general, tracked body size. The three smallest species, a Lemuriform and two species of Callitrix exhibited an accelerated rate of descent in rank. *Cheirogaleus medius* is a heterotherm, and *Callithrix pygmaea* may also be heterothermic (Tattersall, 2012), indicating that the baseline of the logistic function represents a regime of minimal energy reliability, perhaps related to low calorie-density folivory or insectivory.

Following this logic, we can ask what sort of constraint might have been encountered near the plateau of this model, corresponding to the largest relative brain sizes? One likely candidate would be the physiological limit on the rate of heat dissipation (Speakman and Król, 2010; Fromm and Sorger, 2023). During exercise with progressive hyperthermia, human brain temperature increases in parallel with that of the body core, leading to hyperthermia and fatigue (Nybo, 2012; Nybo and Gonález-Alonso, 2015; Tsuji et al, 2016). Contemporary chimpanzee populations that find themselves in the hottest and driest savanna landscapes exhibit thermoregulatory behaviors that likely reduce hyperthermia risk, such as cave use (Lindshield et al, 2021), and over a period spanning 700,000 years of human evolution, body mass and length varied inversely as a function of temperature, suggesting an inherited evolutionary potential to adapt to thermoregulatory demands (Stibel, 2023).

Previously we reported several observations indicating a reciprocal relationship in the evolution of body temperature and metabolic rate: in the case of primates, body temperatures (T_b) were inversely correlated with *mirFam* (Fromm and Sorger, 2023). The conserved nature of this relationship can be visualized by ranking primate species according to the product of *mirFam* x T_b (Supplementary Figure S5). We hypothesized that this product is representative of the heat dissipation limit, and when ordered according to the rate of core thermogenesis (*cMR.53cor*), *mirFam* x T_b tracked thermal conductance (Supplementary Figure S6). In this case, the accelerated evolution detected near the plateau of a

mirFam x T_b logistic model might signal a thermoregulatory adaptation. This appears to be have been the case for the divergence of hominid apes (Figure 9C, D), corresponding to the disproportionate increase in the total mass of the 4-organ core that accompanied the enlargement of the hominid brain and the associated variation in thermal conductance (Supplementary Figure S6).

Bayesian inference predicted opposite evolutionary trends for the evolution of the relationship to brain size of *mirFam* and *mirFam* x T_b: descending in rank on the *mirFam* tree, and ascending in rank on the tree for *mirFam x* T_b (Figure 9). Thus, our logistic model would assign the ancestral primate a high rank with respect to energy reliability and a low rank with respect to the heat dissipation limit, a propitious combination for the founder of a new order of mammals, perhaps situated in the valley of an altered fitness landscape (Duran-Nebreda et al, 2024). As we have previously noted (Fromm and Sorger, 2023), reparametrization of rates of energy consumption in terms of *mirFam*-based *cMR*s reveals an unexpected degree of integration of microRNA complements into the energy economy of homeotherms, the basis of which remains to be explored.

METHODS

Physiological Data

The masses and *rMR*s of the four thermogenic organs were obtained from the dataset of Wang et al (2012), itself mainly derived from the compilation of Navarette et al (2011) (Supplementary Table S1). Values for thermal conductance (C_{min}) were obtained from the dataset of Khaliq et al (2014). For comparison with core organ masses and *cMR*s, we substituted congeneric species from the dataset of Wang et al (2012). Where C_{min} was available for two or more species, we chose the one with the mass closest to the species in the Wang dataset.

MicroRNA Families

Complements of microRNA families were obtained from the most complete assembly for each species using covariance model MirMachine (Umu et al, 2023), trained on the manually-curated database MirGeneDB2.1 (Fromm et al 2021) (Supplementary Tables S1 and S2).

Phylogenetic Trees

Using Mesquite © (2021) we derived ultrametric trees for 51 Euarchontoglires or 24 primates from the phylogenies of Alvarez-Carretero et al (2021) and Shao et al (2023), respectively.

Variable Rate Phenograms

Variable rate trees and ancestral node values were inferred using BayesTraits.V4 (Pagel, 1999; Pagel et al, 2004; Venditti et al, 2011) (software available at www.evolution.rdg.ac.uk). Bayes factors for variable rate trees were computed from the difference between the median of the top 1% likelihoods

and the median likelihood of the trees with lowest 1% sum of changes to branch length (Fromm and Sorger, 2023). Phenograms were generated using Phytools (Revell, 2012).

Statistics

Linear, logistic and partial least squares regressions and normal mixture clustering were carried out and visualized using JMP16 ®. All R^2 values were adjusted for the number of predictors. Phylogenetic linear regressions were carried out using the R: CAPER package (Orme, 2013).

DATA AVAILABILITY

The original data with accompanying references and the results of all analyses referred to in the text are provided in the Supplementary Information (below).

ACKNOWLEDGMENT

BF is supported by the Tromsø forskningsstiftelse (TFS) [20_SG_BF 'MIRevolution'].

AUTHOR CONTRIBUTIONS

Conceptualization: TS; Methodology: TS; Investigation: BF and TS; Writing – Original Draft: TS; Writing – Review & Editing: BF and TS; Visualization: TS; Funding Acquisition: BF.

DECLARATION OF INTERESTS The authors declare no competing interests.

REFERENCES

Aiello LC and Wheeler P. 1995. The expensive-tissue hypothesis: the brain and the digestive system in human and primate evolution. *Curr Anthro* 36: 199 - 221.

Álvarez-Carretero S, Tamuri A, Battini M, Nascimento F, Carlisle E, Asher R, Yang Z, Donoghue P and Dos Reis M. 2022. A species-level timeline of mammal evolution integrating phylogenomic data. *Nature* 602: 263 - 267.

Antol J and Kozlowski J. 2020. Scaling of organ masses in mammals and birds: phylogenetic signal and implications for metabolic rate scaling. *ZooKeys* 982: 149 - 159.

Baek D, Villén J, Shin C, Camargo FD, Gygi SP and Bartel DP. 2008. The impact of microRNAs on protein output. *Nature* 455: 64-72.

Ballesteros FJ, Martinez VJ, Luque B, Lacasa L, Valor E and Moya A. 2018. On the thermodynamic origin of metabolic scaling. *Scientific Reports* 8: 1448.

Bier DM, Leake RD, Haymond MW, Arnold KJ, Gruenke LD, Sperling MA and Kipnis DM. 1977. Measurement of "True" Glucose Production Rates in Infancy and Childhood with 6,6-Dideuteroglucose. *Diabetes* 25: 1016 - 23,

Burger JR, George MA, Leadbetter C and Shaikh F. 2019. The allometry of brain size in mammals. *J Mammal*, 100: 276 - 283.

Buttgereit F and Brand MD. 1995. A hierarchy of ATP-consuming processes in mammalian cells. *Biochem J* 312: 163 -167.

Celeux G and Govaert G. 1995. Gaussian Parsimonious Clustering Models. *Pattern Recognition* 28: 781 - 793.

Chung ST, Chacko SK, Sunehag AL and Haymond MW. 205. Measurements of Gluconeogenesis and Glycogenolysis: A Methodological Review. *Diabetes* 64: 3996 - 4010.

Claassen JAHR, Thijssen DHJ, Panerai RB and Faraci FM. 2021. Regulation of cerebral blood flow in humans: physiology and clinical implications of autoregulation. *Physiol Rev* 101: 1487 - 1559.

Dart, RA. 1925. Australopithecus africanus: the man–ape of South Africa. *Nature* 115, 195 - 199.

Davies TJ, Daru BH, Bezeng BS . . . Bond WJ. 2020. Savanna tree evolutionary ages inform the reconstruction of the paleoenvironment of our hominin ancestors. *Sci Rep* 10: 12430.

de Jong (1993). SIMPLS: An alternative approach to partial least squares regression. *Chemometrics and Intelligent Laboratory Systems* 18: 251 - 263.

Duran-Nebreda S, Bentley RA, Vidiella B, Spiridonov A, Eldredge N, O'Brien MJ and Valverde S. 2024. On the multiscale dynamics of punctuated evolution. *Trends Ecol Evol*: doi.org/10.1016/j.tree.2024.05.003 (1 - 11).

Elia M. Organ and tissue contribution to metabolic rate. 1992. In: Kinney JM, Tucker HN (eds), *Energy metabolism: tissue determinants and cellular corollaries*. pp 61 - 80. (Raven Press, NY).

Felsenstein J. 1985. Phylogenies and the comparative method. *Amer Naturalist* 125: 1 - 15.

Fonseca-Azevedo K and Herculano-Houzel S. 2012. Metabolic constraint imposes a tradeoff between body size and number of brain neurons in human evolution. *PNAS* 109: 18571 - 18576.

Fristoe TS, Burger JR, Balk MA, Khaliq I, Hof C and Brown JH. 2015. Metabolic heat production and thermal conductance are mass-independent adaptations to thermal environment in birds and mammals. *PNAS* 112: 15934 - 15939.

Fromm B, Høye E, Domanska D, Zhong X, Aparicio-Puerta E, Ovchinnikov V, Umu SU, Chabot, PJ, Kang W, Aslanzadeh M, Tarbier M, Mármol-Sánchez E, Urgese G, Johansen M, Hovig E, Hackenberg M, Friedländer MR and Peterson KJ. 2021. MirGeneDB 2.1: toward a complete sampling of all major animal phyla. *Nucl Acids Res* 50: D204 - D210.

Fromm B and Sorger T. 2023. Rapid adaptation of cellular metabolic rate to the microRNA complements of mammals and its relevance to the evolution of endothermy. *iScience*: 108740.

Gallagher D, Belmonte D, Deurenberg P, Wang Z, Krasnow N, Pi-sunyer X and Heymsfield SB. 1998. Organ-tissue mass measurement allows modeling of REE and metabolically active tissue mass. *Am J Physiol* 275: E249 - E258.

Garcia-Rodriguez D and Giménez-Cassina A. 2021. Ketone bodies in the brain beyond fuel metabolism: from excitability to gene expression and cell signaling. *Front Mol Neurosci* 14: 732120.

Grabowski M, Kopperud BT, Tsuboi M and Hansen TF. 2023. Both diet and sociality affect primate brain-size evolution. *Syst Biol* 72: 404 - 418.

Hansen TF. 1997. Stabilizing selection and the comparative analysis of adaptation. *Evolution* 51: 1341 - 1351.

Heldstab SA, Isler K, Graber SM, Schuppli C and van Schaik. 2022. The economics of brain size evolution in vertebrates. *Curr Biol* 32: R697 - R708.

Hubbert MK. 1982. Techniques of prediction as applied to the production of oil and gas. In Gass, Saul I. (ed.) *Oil and Gas Supply Modeling* (proceedings of a symposium held at the Department of Commerce, Washington, DC, June 18–20, 1980). NBS Special Publication 631. Washington (DC): National Bureau of Standards. pp. 16–141.

Isler K and van Schaik CP. 2012. Allomaternal care, life history and brain size evolution in mammals. *J Human Evol* 63: 52 - 63.

Isler K and van Schaik CP. 2014. How humans evolved large brains: comparative evidence. *Evol Anthropol* 23: 65-75.

Khaliq I, Hof C, Prinzinger R, Böhning-Gaese K and Pfenninger M. 2014. Global variation in thermal tolerances and vulnerability of endotherms to climate change. *Proc Roy Soc B* 281: 20141097 (1 - 8).

Kiyatkin AE. 2007. Brain temperature fluctuations during physiological and pathological conditions. *Eur J Appl Physiol* 101: 3 - 17.

Kleiber M. 1932. Body size and metabolism. *Hilgardia* 6: 315 - 353.

Koteja P. 2000. Energy assimilation, parental care and the evolution of endothermy. *Proc Roy Soc B* 267: 479 - 484.

Kuderna LFK, Gao H, Janiak MC . . . Bonet TM. 2023. A global catalog of whole-genome diversity from 233 primate species. *Science* 380: 9 - 913.

Kummitha CM, Kalhan SC, Saidel GM and Lai N. 2014. Relating tissue/organ energy expenditure to metabolic fluxes in mouse and human: experimental data integrated with mathematical modeling. *Physiol Rep* e12159 (1 - 20).

Kuzawa CW, Chugani HT, Grossman LI, Lipovich L, Muzik O, Hof PR, Wildman DE, Sherwood CC, Leonard WR and Lange N. 2014. Metabolic costs and evolutionary implications of human brain development. *PNAS* 111: 13010 - 13015.

Lande R. 1979. Quantitative genetic analysis of multivariate evolution, applied to the brain: body size allometry. *Evolution* 33: 402 - 416.

Magalhães JP, Abidi Z, dos Santos GA . . . Ka Po To P. 2024. Human Ageing Genomic Resources: updates on key databases in ageing research. *Nucl Acids Res* 52: D900 - D908.

Lindshield S, Hernandez-Aguilar RA, Korstjens AH . . . Yoshikawa M. 2021. Chimpanzees (*Pan troglodytes*) in savanna landscapes. *Evol Antropol* 30: 399 - 420.

Mascia-Lees FE, Relethford JH and Sorger T. 1986. Perspectives on permanent breast enlargement in human females. *Amer Anthro* 88: 423 - 428.

Navarette A, van Schaik CP and Isler K. 2011. Energetics and the evolution of human brain size. *Nature* 480: 91 - 93.

Naya DE, Spangenberg L, Naya H and Bozinovic F. 2013. Thermal conductance and basal metabolic rate are part of a coordinated system for heat transfer regulation. *Proc Roy Soc B* 280: 20131629.

Notley SR, Mitchell D and Taylor NAS. 2024. A century of exercise physiology: concepts that ignited the study of human thermoregulation. Part 4: evolution, thermal adaptation and unsupported theories of thermoregulation. *Eur J Appl Physiol* 124: 147 - 218.

Nybo L. 2012. Brain temperature and exercise performance. *Exp Physiol* 97: 333 - 339.

Nybo L, Secher NH and Nielsen B. 2002. Inadequate heat release from the human brain during prolonged exercise with hyperthermia. *J Physiol* 545: 697 - 704.

Nybo L and González-Alonso J. 2015. Critical core temperature: a hypothesis too simplistic to explain hyperthermia-induced fatigue. *Scand J Med Sci Sports* 25: 4 - 5.

Orme D, Freckleton RP, Thomas GH and Petzoldt T. 2013. CAPER: comparative analyses of phylogenetics and evolution in R. *Methods Ecol and Evol* 3: 141 - 151.

Owen OE, Morgan AP, Kemp HG, Sullivan JM, Herrera MG and Cahill GF. 1967. Brain metabolism during fasting. *J Clin Inv* 46: 1589 - 1595.

Pagel M. 1999. Inferring the historical patterns of biological evolution. *Nature* 401: 877 - 884.

Pagel M, Meade A and Barker D. 2004. Bayesian estimation of ancestral character states on phylogenies. *Syst Biol* 53: 673 - 684.

Paine OCC, Koppa A, Henry AG . . . Sponheimer M. 2019. Seasonal and habitat effects on the nutritional properties of savanna vegetation: Potential implications for early hominin dietary ecology. *J Hum Evol* 133: 99 - 107.

Pontzer H, Brown MH, Raichlen DA . . . Ross SR. 2016. Metabolic acceleration and the evolution of human brain size and life history. *Nature* 533: 390 - 393.

Porter WP and Kearney M. 2009. Size, shape, and thermal niche of endotherms. *PNAS* 106: 19666 - 19672.

Reed KE. 1997. Early hominid evolution and ecological change through the African Plio-Pleistocene. *J Hum Evol* 32: 289 - 322.

Revell LJ. 2012. phytools: an R package for phylogenetic comparative biology (and other things). *Methods Ecol Evol* 3: 217 - 223.

Scholander PF, Hock F, Walters V, Johnson F and Irving L. 1950. Heat Regulation in Some Arctic and Tropical Mammals and Birds. *Biol Bull* 99: 237 - 258.

Selbach M, Schwanhäusser B, Thierfelder N, Fang Z, Khanin R, Rajewsky N. 2008. Widespread changes in protein synthesis induced by microRNAs. *Nature* 455: 58–63.

Shao Y, Zhou, Li F . . . Wu DD. 2023. Phylogenomic analyses provide insights into primate evolution. *Science* 380: 913 - 924.

Simmen B, Pasquet P, Masi S, Koppert GJA, Wells JCK and Hladik CM. 2017. Primate energy input and the evolutionary transition to energy-dense diets in humans. *Proc Roy Soc B* 284: 20170577.

Smaers JB, Rothman RS, Hudson DR, Balanoff AM, Beatty B, Dechmann DKN, deVries D, Dunn, JC, Fleagle JG, Gilbert CC, Goswami A, Iwaniuk AN, Jungers WL, Kerney M, Ksepka DT, Manger PR, Mongle CS, Rohlf FJ, Smith NA, Soligo C, Weisbecker V and Safi K. 2021. The evolution of mammalian brain size. *Sci Adv* 7: eabe2101 (1 - 11).

Speakman JR and Król E. 2010. Maximal heat dissipation capacity and hyperthermia risk: neglected key factors in the ecology of endotherms. *J Anim Ecol* 79: 726 – 746.

Staubwasser M, Drăgusin V, Onac BP, Assonov S, Ersek V, Hoffmann DL and Veres D. 2018. Impact of climate change on the transition of Neanderthals to modern humans in Europe. *PNAS* 115: 9116 – 9121.

Stibel JM. 2023. Climate change is predictive of body size and proportionality in humans. *Evol Biol* 50: 461 - 475.

Sunehag AL, Treuth MS, Toffolo G, Butte NF, Cobelli C, Bier DM and Haymond MW. 2001. Glucose production, gluconeogenesis, and insulin sensitivity in children and adolescents: an evaluation of their reproducibility. *Ped Res* 50: 115 - 123.

Sunehag AL, Toffolo G. Treuth MS, Butte NF, Cobelli C, Bier DM and Haymond MW. 2002. Effects of dietary macronutrient content on glucose metabolism in children. *J Clin Endocrin Metab*l 87: 5168 - 5178.

Svensson EI, Arnold SJ, Bürger R et al. 2021. Correlational selection in the age of genomics. *Nat Ecol Evol* 5, 562–573.

Tattersall GJ. 2012. Diurnal changes in metabolic rate in pygmy marmosets: Implications for sleep, torpor, and basal metabolism in primates. In: Ruf, T., Bieber, C., Arnold, W., Millesi, E. (eds) *Living in a Seasonal World*, chapter 41: 471 - 480. Springer.

Timmermann A, Yun KS, Raia P . . . Ganopolski. 2022. Climate effects on archaic human habitats and species succession. *Nature* 604: 495 - 501.

Travers T, Kippelen P, Trangmar SJ and González-Alonzo J. Physiological function during exercise and environmental stress in humans—an integrative view of body systems and homeostasis. *Cells* 11: 383.

Tsuji B, Hayashi K, Kondo N and Nishiyasu T. 2016. Characteristics of hyperthermia-induced hyperventilation in humans. *Temperature* 3: 146 - 160.

Umu SU, Paynter VM, Trondsøn H, Buschmann T, Rounge TB, Peterson KJ and Fromm B. 2023. Accurate microRNA annotation of animal genomes using trained covariance models of curated microRNA complements in MirMachine. *Cell Genomics* 3: 100348.

Venditti C, Meade A. and Pagel M. 2011. Multiple routes to mammalian diversity. *Nature*, 479, 393 - 396.

Walter GM and McCuigan K. 2023. Phenotypic evolution: predicting the future. *eLife* 12: e91450 (1 - 3).

Walters TJ, Ryan KL and Constable SH. 2004. Thermoregulation by rhesus monkeys at different absolute humidities. *J Comp Physiol B* 174: 481 - 487

Wang H, Wang B, Normoyle K, Jackson K, Spitler K, Sharrock MF, Miller CM, Best C, Llano D and Du R. 2014. Brain temperature and its fundamental properties: a review for clinical neuroscientists. *Front Neurosci* 307: 1 - 17.

Wang ZM, Zhang J, Ying Z and Heymsfield SB. 2012. Organ-tissue level model of resting energy expenditure across mammals: new insights into Kleiber's Law. *ISRN Zool*: 673050 (1 - 9).

White CR, Marshall DJ, Alton LA, Arnold PA, Beaman JE, Bywater CL, Condon C, Crispin TS, Janetzki A, Pirtle E, Winwood-Smith HS, Angilletta MJ, Chenoweth SF, Franklin CE, Franklin CE, Halsey LG, Kearney MR, Portugal SJ and Ortiz-Barrientos D. 2019.
The origin and maintenance of metabolic allometry in animals. *Nature Ecol Evol* 3: 598-603.

Wold, S., Johansson, E. and Cocchi, M., 1993. PLS: partial least squares projections to latent structures. In 3D QSAR in *Drug Design: Theory, Methods and Applications*. (pp. 523-550). Kluwer ESCOM Science Publisher.

Zeller E, Timmermann A, Yun KY, Raia P, Stein K and Ruan J. 2023. Human adaptation to diverse biomes over the past 3 million years. *Science* 380: 604 - 608.

SUPPLEMENTARY INFORMATION

Clade	Wang Taxon Names	Names on Phylogeny	*mirFam*	*Mkdn* (g)	*Mhrt* (g)	*Mlvr* (g)	*Mbrn* (g)	*Mcor* (g)	*Mbdy* (g)	*MRkdn* (W)	*MRhrt* (W)	*MRlvr* (W)	*MRbrn* (W)	*MRcor* (W)	*MRbdy* (W)
Primates	*Alouatta sara*	*Alouatta palliata*	174	9.9	24	81.2	56.5	171.6	4399.6	13.7088	13.6112	33.6452	12.9948	73.96	169.5872
Primates		*Callithrix jacchus*	172	2.9	2.8	17.8	7.3	30.8	311.8	6.039	17.928	37.352	20.453	81.772	180.7072
Primates	*Cebualla pygmaea*	*Callithrix pygmaea*	171	1.9	0.86	13.5	4.4	20.66	162.66	6.8432	11.1622	29.0377	20.9296	67.9727	112.3625
Primates		*Cheirogaleus medius*	176	1	0.93	6.3	2.8	11.03	231.03	1.5238	0.94858	15.012	2.5432	20.02758	25.77858
Primates		*Chlorocebus pygerythrus*	199	12.1	42.6	89	80.8	224.5	5300.5	2.204	2.8616	16.643	3.8471	25.5557	35.7841
Primates		*Colobus guereza*	198	23.3	37	171	86.5	317.8	9749.8	2.9356	3.5644	14.553	6.2832	27.3362	46.7808
Primates		*Eulemur fulvus*	180	9.5	11.8	43.4	22.5	87.2	2500.2	1.4364	3.3495	13.248	4.0794	22.1133	33.0213
Primates		*Eulemur macaco*	180	14.2	9.1	77.8	24.2	125.3	1875.3	2.2227	3.4817	16.2184	4.78	26.7028	45.6892
Primates	Human	*Homo sapiens*	208	250	320	1700	1300	3570	59970	9.2862	14.1312	40.05	25.56	89.0274	199.0161
Primates	*Hylobates concolor*	*Hylobates pileatus*	195	35.2	58.2	293	137.8	524.2	6550.2	13.3043	25.16	63.612	27.9395	130.0158	323.3718
Primates		*Lemur catta*	178	11.2	11.7	72.9	22.8	118.6	2074.6	12.789	17.135	50.27	15.162	95.356	195.6392
Primates		*Leontopithecus chrysomelas*	173	4.1	3.8	18.9	13.2	40	642	27.4	39.162	78.566	35.518	180.646	471.706
Primates	*Macaca nigra*	*Macaca arctoides*	205	50	61	241	118	470	15870	42.6393	63.242	115.64	49.59	271.1113	669.3613
Primates	Monkey	*Macaca fascicularis*	207	21	23	110	42	196	4500	21.394	51.5696	84.252	44.5244	201.74	419.94
Primates		*Mandrillus sphinx*	194	49.9	76	331	168	624.9	23024.9	0.8932	1.31274	3.9304	2.006	8.14234	13.62034
Primates		*Papio hamadryas*	197	80.3	103	392	174	749.3	23249.3	2.229	2.4725	9.2769	3.8025	17.7809	31.2792
Primates	*Saguinus lagonotus*	*Saguinus midas*	170	1.9	3.3	14.4	7.8	27.4	330.4	0.2841	0.2094	2.2764	0.56832	3.33822	4.47022
Primates		*Saguinus oedipus*	172	3.1	3.7	20.9	10	37.7	623.7	0.23424	0.1456	1.39829	0.2828	2.06093	2.90093
Primates		*Saimiri boliviensis*	174	6.7	6.5	19.4	29	61.6	1002.6	0.609	0.34636	3.7466	0.7304	5.43236	8.15126
Primates		*Sapajus apella*	171	10.4	13.4	49.3	50.8	123.9	1749.9	0.5126	0.25916	3.4181	0.29133	4.48119	5.79399
Primates		*Symphalangus syndactylus*	194	43.7	51.5	294	143	532.2	8500.2	1.179	0.93177	9.5588	1.2834	12.95297	20.57737
Primates		*Theropithecus gelada*	203	38	77.2	236	140.9	492.1	11402.1	0.27412	0.10241	1.43344	0.29232	2.10229	2.94789
Primates		*Trachypithecus vetulus*	197	15.4	19.2	90	72	196.6	4999.6	0.47379	0.21728	3.2058	0.3715	4.26837	5.62837
Primates		*Varecia rubra*	181	22.4	18.1	72.2	35.7	148.4	4200.4	0.25038	0.19992	2.1967	0.44973	3.09673	4.03113
Scandentia		*Tupaia glis*	151	1.1	1.17	3.4	3.4	9.07	141.07	0.31892	0.24768	1.835	0.46055	2.86215	4.13635
Glires		*Acomys minous*	157	0.32	0.18	0.9	0.9	2.3	42.3	0.779	0.98487	6.3756	1.54	9.67947	18.10547
Glires		*Apodemus flavicollis*	141	0.34	0.18	1	0.61	2.13	25.13	7.2688	9.5589	41.0427	9.1884	67.0588	118.8928
Glires		*Apodemus sylvaticus*	155	0.26	0.14	1.1	0.57	2.07	18.07	6.0705	9.4282	23.219	8.82	47.5377	109.5518
Glires		*Arvicola sapidus*	149	0.7	0.28	2.6	1.1	4.68	61.68	9.301	7.5257	44.9684	9.8736	71.6687	118.9187
Glires	Guinea Pig	*Cavia porcellus*	174	5.6	2.3	27	4.7	39.6	799.6	4.623	5.785	13.2502	12.934	36.5922	64.7281
Glires		*Gerbillus perpallidus*	147	0.27	0.13	1	0.58	1.98	29.98	110	140.8	340	312	902.8	1489.36
Glires		*Glaucomys volans*	176	0.59	0.56	2.9	1.9	5.95	54.95	20.768	41.4966	121.302	47.1276	230.6942	362.6636
Glires		*Glis glis*	168	0.68	0.48	3.2	1.5	5.86	83.86	25.2149	35.5865	113.484	47.047	221.3324	388.6604
Glires		*Jaculus jaculus*	158	0.29	0.45	1.1	1.2	3.04	48.04	7.26	31.1406	38.982	28.4416	105.8242	221.0494
Glires		*Lepus europaeus*	173	18.5	28.9	90.4	14.8	152.6	3338.6	26.4969	46.74	97.645	48.048	218.9299	617.6499
Glires		*Microtus agrestis*	148	0.17	0.12	0.63	0.39	1.31	15.31	11.544	22.3108	44.748	5.5648	84.1676	162.2246
Glires		*Microtus arvalis*	153	0.55	0.19	1.9	0.39	3.03	27.03	4.3533	4.2864	22.048	3.5392	34.2269	61.949
Glires		*Microtus pinetorum*	154	0.36	0.15	1.1	0.58	2.19	21.19	0.57664	0.57312	4.256	0.954	6.35976	9.89316
Glires		*Mus musculus*	167	0.28	0.07	0.68	0.36	1.39	15.39	0.67473	0.76758	3.6366	1.4784	6.55731	10.79621
Glires	Mouse	*Mus musculus domesticus*	167	0.51	0.16	1.8	0.5	2.97	27.97	0.51802	0.70224	4.3094	1.2825	6.81216	9.19356
Glires		*Myodes glareolus*	143	0.24	0.1	0.67	0.35	1.36	15.36	1.3056	1.7629	5.3185	3.3831	11.7701	21.4049
Glires		*Octodon degus*	156	1.1	0.41	4.8	1.9	8.21	129.21	2.304	2.6488	12.8904	3.6075	21.4507	39.9589
Glires		*Peromyscus leucopus*	160	0.3	0.15	1.2	0.74	2.39	22.39	0.8998	0.46494	5.6736	1.1343	8.17264	13.26674
Glires		*Rattus norvegicus*	168	1.5	0.87	9.2	2.3	13.87	209.87	3.9368	2.1022	19.602	2.1667	27.8077	51.4437
Glires	Rat	*Rattus rattus*	167	2.8	1.1	14.3	1.9	20.1	390.1	0.25752	0.57375	1.6973	0.8256	3.35417	5.59067
Glires		*Rhabdomys pumilio*	161	0.41	0.21	1.8	0.6	3.02	50.02	0.28704	0.23274	1.4337	0.63	2.58348	4.61148
Glires		*Sciurus carolinensis*	175	3.2	2.8	16.4	7.5	29.9	595.9	0.34272	0.21075	2.1175	0.44892	3.11989	4.20479
Glires		*Sciurus niger*	165	3	2.5	10.7	7.5	23.7	412.7	0.16592	0.17472	1.31481	0.31512	1.97057	2.81057
Glires		*Sciurus vulgaris*	175	1.7	1.7	5.5	6.3	15.2	274.2	0.24948	0.17511	1.748	0.4263	2.59889	4.10249
Glires		*Sylvilagus floridanus*	170	6.3	4.8	32	7.9	51	972	2.0888	1.0945	12.584	0.9709	16.7382	29.7252
Glires		*Tamias striatus*	173	0.81	0.66	2.9	2.4	6.77	103.77	0.36285	0.26607	2.7414	0.4098	3.78012	6.09722

Table S1. Summary of species *mirFam*, mass and resting metabolic rates for organs, core and body. All physiological data were obtained from Wang et al (2012), most of which were compiled by Navarette et al (2011). The names of the indicated taxa were substituted with congeneric species on the phylogenies of Álvarez-Carretero et al (2022) and Shao et al (2023).

Order	Species	*mirFam*	ECV	Mass (g)	T_b (°C)
Catarrhini	*Homo sapiens*	208	1252.00	50000	37.0
Catarrhini	*Pan troglodytes*	206	368.35	44967	35.7
Catarrhini	*Gorilla gorilla*	202	490.41	120950	35.5
Catarrhini	*Macaca fascicularis*	207	63.98	4251	37.6
Catarrhini	*Macaca mulatta*	208	88.98	6793	37.3
Catarrhini	*Papio hamadryas*	197	146.17	14150	38.0
Catarrhini	*Chlorocebus aethiops*	199	65.00	3720	36.8
Catarrhini	*Erythrocebus patas*	201	97.73	9450	39.3
Catarrhini	*Cercopithecus mitis*	200	71.33	6109	37.5
Catarrhini	*Colobus guereza*	198	74.39	8589	37.0
Platyrrhini	*Callithrix jacchus*	172	7.24	320	36.0
Platyrrhini	*Callithrix pygmaea*	171	4.17	116	35.2
Platyrrhini	*Aotus trivirgatus*	177	16.85	989	38.0
Platyrrhini	*Saimiri sciureus*	174	24.14	799	38.0
Platyrrhini	*Alouata palliata*	174	49.88	6250	36.0
Lemuriformes	*Eulemur fulvus*	180	25.77	2292	36.5
Lemuriformes	*Cheirogaleus medius*	176	2.60	140	38.0
Lemuriformes	*Propithecus verreauxi*	180	26.21	2955	36.0
Lorisiformes	*Otolemur garnettii*	166	11.50	764	36.0
Lorisiformes	*Otolemur crassicaudatus*	166	11.78	1150	36.6
Lorisiformes	*Galago senegalensis*	165	3.96	194	37.9
Lorisiformes	*Loris tardigradus*	166	5.87	193	35.5
Lorisiformes	*Nycticebus coucang*	167	10.13	653	35.4
Lorisiformes	*Arctocebus calabarensis*	166	6.92	309	36.0
Lorisiformes	*Perodicticus potto*	169	12.42	835	35.4

Table S2. Summary of *mirFam*, brain volume (ECV), body mass and temperature among primates. Endocranial volume (ECV) and body mass were obtained from Grabowski et al (2023). Body temperatures were obtained from the AnAge database (Magalhães et al, 2024).

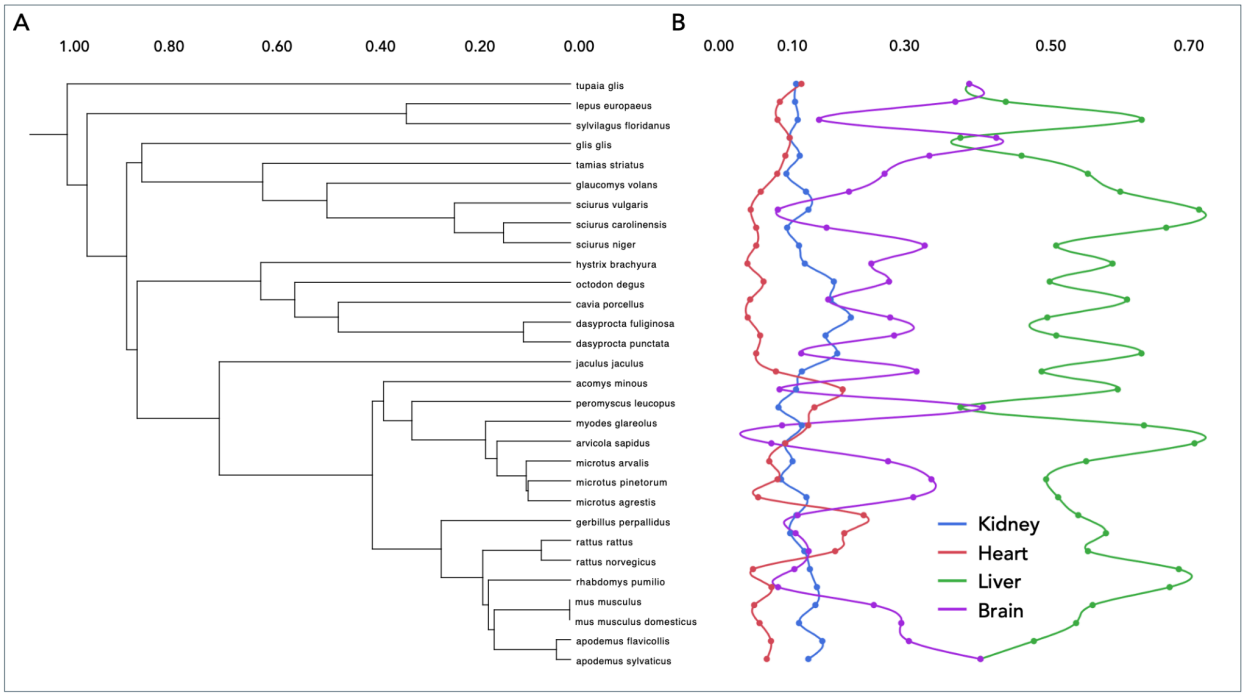

Figure S1. The proportions of brain and liver vary reciprocally in the Euarchontoglires core. Species include one Scandentia, two Lagomorpha, and 27 Glires, including three Sciuridae.
A. Ultrametric phylogenetic tree. The scale bar represents relative time of divergence.
B. Mass proportion of each organ relative to the total core mass.

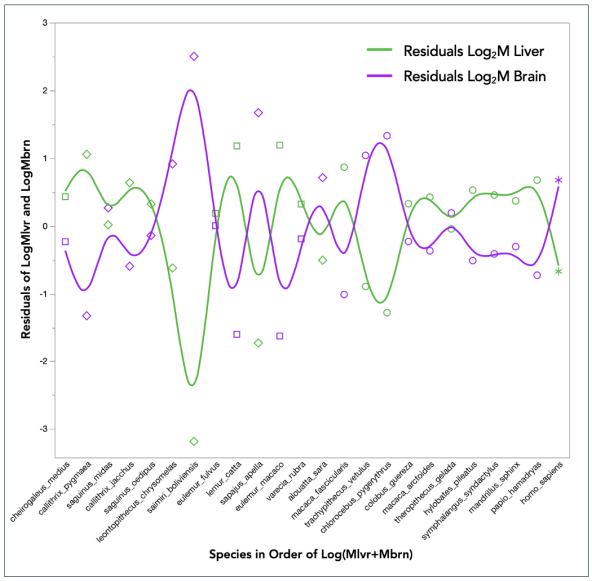

Figure S2. Tradeoffs between primate liver and brain as a function of their combined mass. The “phase shift” between the residuals of liver and brain with respect to the core (Figure 4D) can be isolated by repeating the regression with respect to Log (*Mlvr* + *Mbrn*), demonstrating that the periodicity depends on autocorrelation.

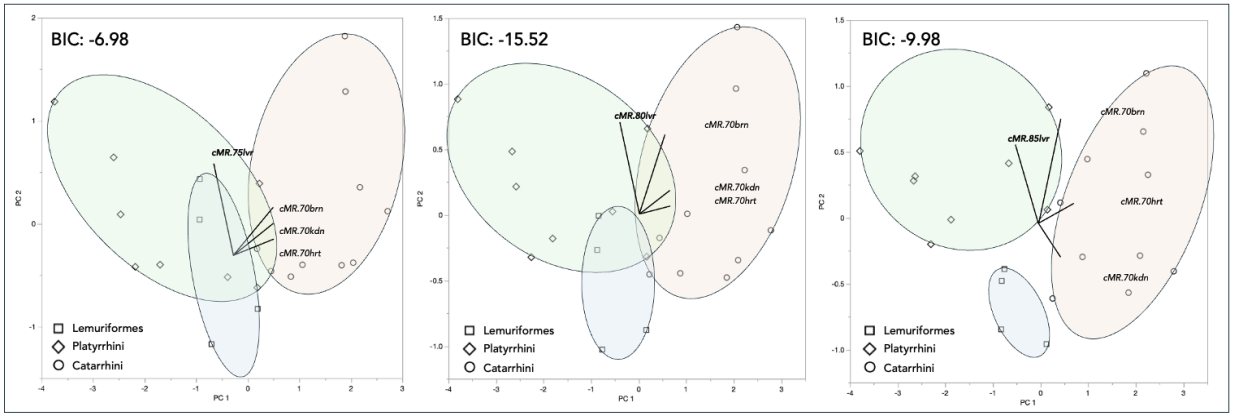

Figure S3. Unsupervised classification of primate clades based on core *cMR* composition. Principal components were calculated from each *cMR* correlation matrix, and membership in two clusters estimated by expectation maximization of their joint probability distributions. Kidney, heart and brain *cMR* = *cMR.70*; liver *cMR*s were varied between *cMR.75lvr* - *cMR.85lvr* (bold type). Ellipses were hand-drawn to include all members of the three phylogenetic clades (N = 22).

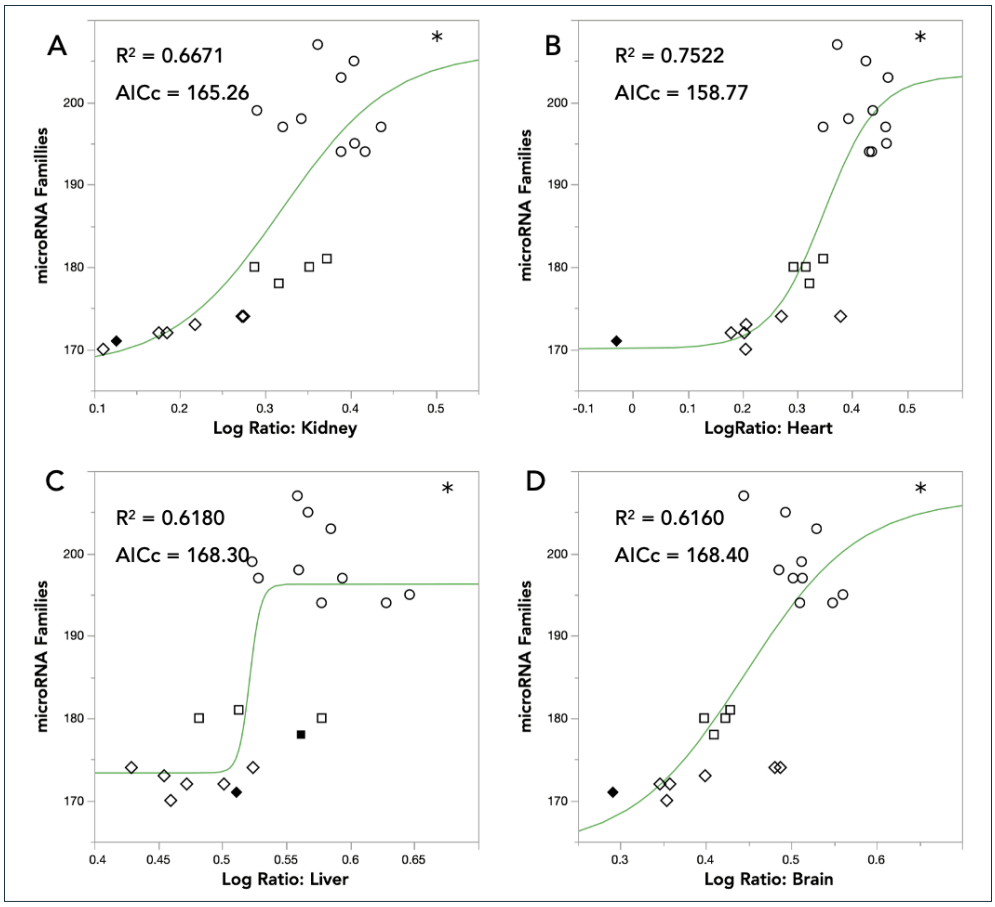

Figure S4. Logistic models for evolution of the relative size of four thermogenic organs. Symbols representing clades as in previous figures, with filled symbols representing heterotherms.

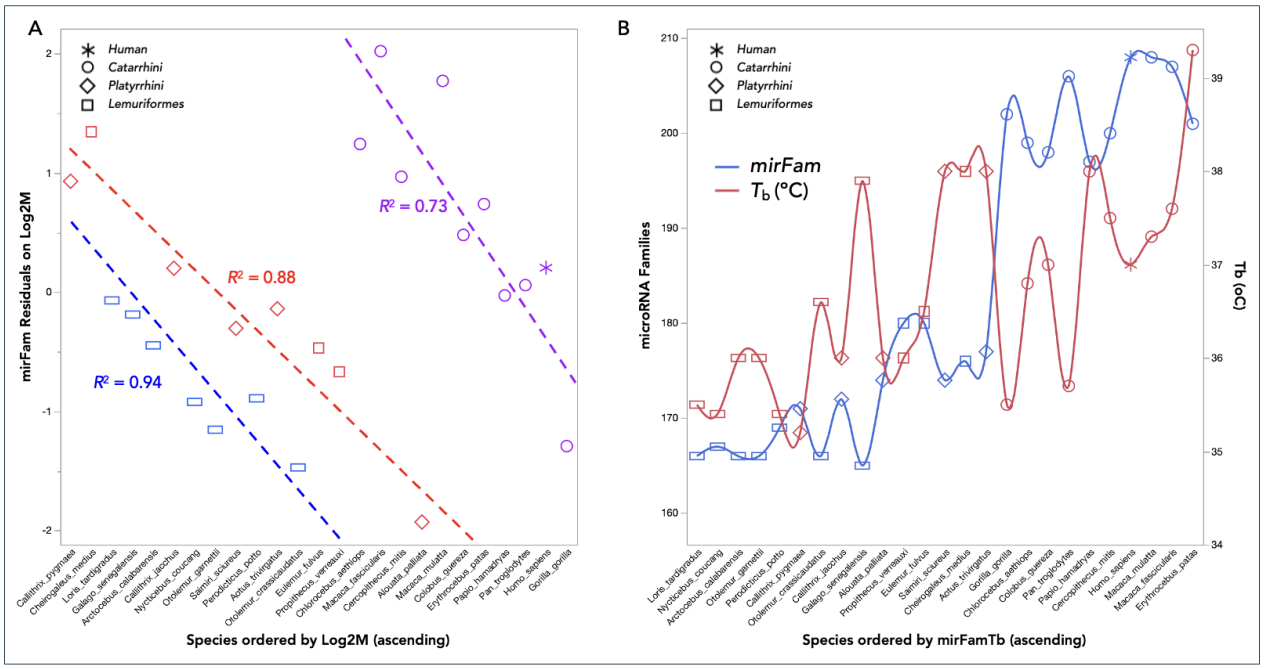

Figure S5. Conservation of *mirFam* and *mirFam* x T_b.
A. The *mirFam*-$\log_2 M$ relationship is least conserved among Catarrhini (purple).
B. Visualization of the reciprocal variation of *mirFam* and T_b.

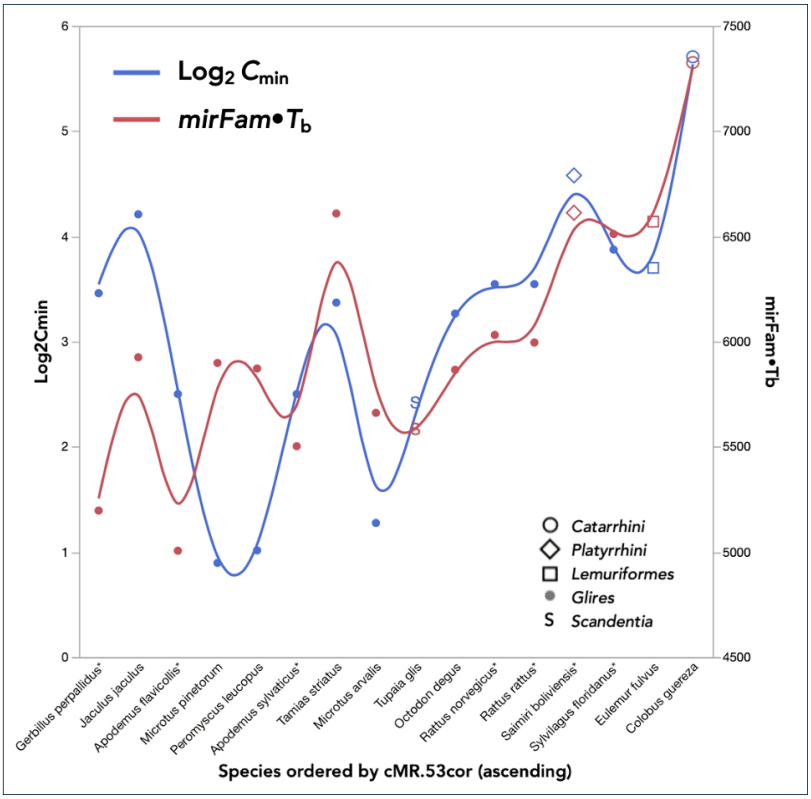

Figure S6. When ordered according to the rate of core thermogenesis (*cMR.53cor*), *mirFam*•T_b (red) generally tracks thermal conductance (blue).
Asterisks (*) indicate species in the 4-organ dataset of Wang et al (2012) that were substituted for congeneric species in the C_{min} dataset of Khaliq et al (2014).

	Allometric Exponent	Pagel's *lambda*	R^2	*P*	*AICc*
KIDNEY	0.80	0	0.5366	6.39E-05	-42.7
	0.75	0	0.5834	2.14E-05	-20.09
	0.70	0	0.5958	1.56E-05	-0.93
	0.65	0	0.5946	1.61E-05	16.22
	0.60	0	0.5859	2.00E-05	32.13
		Pagel's *lambda*	R^2	*P*	*AICc*
HEART	0.80	0	0.4937	1.60E-04	-38.02
	0.75	0	0.6476	3.83E-06	-17.88
	0.70	0	0.6962	8.44E-07	0.63
	0.65	0	0.7133	4.69E-07	17.65
	0.60	0	0.7163	4.21E-07	33.66
		Pagel's *lambda*	R^2	*P*	*AICc*
LIVER	0.80	0	0.5724	2.79E-05	-15.22
	0.75	0	0.4011	9.28E-04	-10.98
	0.70	0	0.0854	1.01E-01	-2.86
	0.65	0	-0.0344	5.89E-01	10.24
	0.60	0.962	0.0145	2.66E-01	27.34
		Pagel's *lambda*	R^2	*P*	*AICc*
BRAIN	0.80	1	0.0329	2.05E-01	-63.9
	0.75	1	0.107	7.55E-02	-35.75
	0.70	1	0.1336	5.07E-02	-10.58
	0.65	1	0.151	4.17E-02	11.76
	0.60	1	0.1596	3.71E-02	32.24

Supplementary Table S3. Summary of phylogenetic regressions of primate organ *cMR*s on *mirFam*. For reference, see the logistic regressions of *mirFam* on relative organ size (Figure S4).